

pubs.acs.org/JPCC Article

A Holstein-Peierls Approach to Excimer Spectra: The Evolution from Vibronically Structured to Unstructured Emission

Published as part of The Journal of Physical Chemistry virtual special issue "Quantum Coherent Phenomena in Energy Harvesting and Storage".

April L. Bialas and Frank C. Spano*



Cite This: J. Phys. Chem. C 2022, 126, 4067-4081



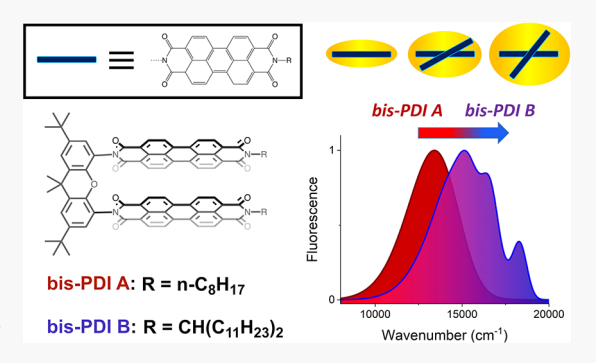
ACCESS

Metrics & More

Article Recommendations

s Supporting Information

ABSTRACT: The presence of excimers, as revealed by broad, structureless, and red-shifted emission, is quite common in a great many organic solutionand solid-phase systems. A fundamental theoretical account of excimer creation and relaxation has generated enormous interest over the years. Here, a model based on a Holstein—Peierls Hamiltonian is presented to account for absorption and photoluminescence in molecular dimers. The model extends the Frenkel-charge transfer (CT)-Holstein model in order to account for both local and nonlocal coupling to a slow *inter*molecular vibrational mode. The model shows that excimer emission can be induced either through (1) local *inter*molecular coupling to the dimer CT states or through (2) the nonlocal Frenkel-CT coupling terms. Finally, by incorporating *both* the local and nonlocal *inter*molecular coupling, the



measured absorption and excimer emission spectra for a set of two different bis(perylene diimide) covalently linked dimers are successfully reproduced. The evolution from structured to unstructured excimer emission likely occurs via an increase in the nonlocal coupling, but it can also be induced by the stabilization of the diabatic CT state.

■ INTRODUCTION

In 1955, Förster and Kasper, followed by Birks and coworkers in the 1960s, pioneered spectroscopic studies on pyrene in *solution* in order to better understand the mechanism of the broad, structureless, Stokes-shifted peak that occurs only in the fluorescence, but not absorption, spectrum upon increasing concentration. This same characteristic fluorescent signature is observed in a variety of other small organic π -stacked dimers and has been commonly termed an "excimer," as was first coined by Stevens et al. in 1960 in order to describe a dimer which is only stabilized in its excited state. However, the term has been widely extended to describe similarly classified peaks that also occur in the *crystal* phase of π -stacked small organic chromophores.

Solution- and crystal-phase excimers are believed to be of similar origin due to the strong overlap of the fluorescence spectrum of a highly concentrated solution with the spectrum of a crystal. The broad, structureless, red-shifted features of the excimer are commonly attributed to a structural reorganization from an initial excited state to a more stable, bound excited state, from which emission occurs to a repulsive ground state potential. The dissociative ground state potential in the original model was approximated using two interacting neutral spheres, a model that becomes even more approximate when neglecting attractive van der Waals forces and favorable

interactions in a crystal environment.¹¹ However, as pointed out previously, excimer-like shifts can still arise from a bound ground-state potential, where broadening arises from the inclusion of intermolecular vibrations.^{12,13}

While each state's relative oscillator strength competes in the steady-state absorption spectrum, emission commonly occurs from the lowest energy excited states and therefore fluorescence spectra can originate from a variety of different geometries, ranging from the ground-state to deformed or excited-state configurations. Overall, the literature commonly agrees that excimer formation involves structural relaxation along an *inter*molecular coordinate toward a geometry that exhibits larger π -orbital overlap, typically within a picosecond time scale for perylene diimide (PDI) dyes. 11,14 Excimers have been demonstrated to arise from exciton-like precursors on a picosecond time scale, where the final excimeric state can further relax preceding a nanosecond radiative decay. 15,16 It is therefore often assumed under the adiabatic approximation

Received: December 2, 2021 Revised: January 17, 2022 Published: February 16, 2022





that steady-state emission dominantly occurs from the "excimer geometry" or from a relaxed excited-state geometry; ¹³ however, some theoretical approaches attribute excimer signatures to an average emission over several different geometries. ^{17,18}

Original studies involving crystalline pyrene had suggested that the low-energy fluorescence peak arises from a) dipole—dipole interactions⁵ or b) charge transfer transitions;¹⁹ however, subsequent theories supported excimer states arising from Frenkel exciton and charge transfer (CT) exciton mixing in a relaxed *inter*molecular geometry.^{5,10,12,20–22} Recently, Wasielewski et al. postulated an upper and lower threshold for the magnitude of the Frenkel-CT coupling required for excimer formation;²³ however, an intuitive physical justification is lacking, highlighting the need to better understand the role of CT states in excimer evolution.

Most excimer fluorescence spectra are recorded at room temperature, where emission no longer occurs from only the lowest energy state. The pioneering work of Birks and coworkers first determined that excimer formation of pyrene in *solution* is diffusion-controlled, concentration-dependent, and reversible.^{2–4} Some experiments show a relative decrease of the excimer peak accompanied by an increase in monomer fluorescence with temperature, presumably as the dimer dissociates.^{9,10,24,25}

Oddly, some experiments observe structured excimer peaks in solution, even after subtracting out monomer emission. 13,26 Furthermore, even in the crystal-phase, some experiments reveal a competition between conventional excimer emission and exciton (or monomer-like) structured emission, 27,28 while in other studies, excimer emission appears dominant.^{29,30} However, in a crystal lattice or in a rigid covalently linked dimer such as that in Figure 8 (see section Comparison to Experiment), the "monomer" emission peak becomes more difficult to justify. In some cases, a blue-shifted vibronically structured peak grows in with temperature, which has been attributed to a lower exciton peak³¹ or the emergence of a freeexciton band.³² Recently, temperature-dependent emission studies on a PDI foldamer revealed that in one solvent both the excimer and the "monomer"-like signatures increase in intensity as a function of temperature, 28 a trend that contradicts an interpretation based on an equilibrium between monomer and foldamer (dimer) phases. While excimer emission remains commonplace in many systems, the detailed nature of excimers remains theoretically elusive.

Formerly, exciton models have not been considered suitable for describing excimer formation due to their neglect of *inter*molecular vibrational modes, and therefore, *ab initio* dimer methods have been the favored theoretical approach.^{13,33} Some drawbacks to relying on *ab initio* methods to implement the *inter*molecular behavior in the emission is that the inclusion of many atoms and vibrations is computationally expensive, while obtaining accurate relative CT and Frenkel states remains quite theoretically challenging.³⁴

Previous approaches including local vibronic coupling via Holstein-style Frenkel-CT Hamiltonians have been successful in simulating fluorescence spectra with clear *intra*molecular vibronic progressions (effective modes on the order of 1400 cm⁻¹).³⁵⁻³⁷ In this paper, we expand the Hamiltonian to include also local and nonlocal (i.e., Peierls-like) coupling involving a slow, torsional mode, such as that pioneered by Silbey and Munn,³⁸ in order to describe excimer emission. In our approach, exciton states, CT states, *intra*molecular

vibrations, and *inter*molecular vibrations are all treated on equal footing in order to simulate both absorption and emission, which, to the best of our knowledge, has not been done previously. The use of a simple model helps to clarify the minimum physical requirements to observe excimer emission, and can powerfully point to spectroscopic trends as a function of a small set of physical parameters, at a smaller computational cost.

The model proposed in this work gives insight into the role that Frenkel excitons, CT states, *intra*molecular vibrations, and *inter*molecular vibrations all play in the formation of excimer emission in dimers of small organic chromophores. We find that excimer signatures can be induced by either (1) local coupling of the dimer CT states to an effective *inter*molecular vibrational mode or (2) nonlocal coupling, in which the *inter*molecular vibrational mode modulates the coupling between the Frenkel and CT states. However, both local and nonlocal coupling are required to successfully simulate experimental spectra with reasonable parameters. Our model suggests that the excimer states have a large charge transfer character, which is consistent with the small transition dipole moments and long lifetimes observed in many experimental studies of excimers. ^{29,39,40}

In what follows, we consider the absorption and emission spectra of two bis-PDI dyes presently referred to as bis-PDI-A and bis-PDI-B, taken from ref 41. Bis-PDI-A displays a conventional broad, structureless, and Stokes-shifted excimer emission, while bis-PDI-B exhibits an unstructured broad excimer peak at lower energy, but with a structured intramolecular vibronic progression of a 1400 cm⁻¹ mode at higher energies, typical signatures of either monomer emission or emission from Frenkel excitons coupled to intramolecular vibrations. We find that weaker nonlocal couplings, at reasonable CT energies, generate a composite fluorescence spectrum that exhibits both structured and unstructured components whereas stronger nonlocal coupling, or further stabilization of the diabatic CT state, further Stokes shifts the excimer peak until no intramolecular vibronic structure is achieved at room temperature. In a simplified picture, the structured components can be attributed to having more Frenkel-exciton character whereas the unstructured components arise from the strong intermolecular coupling to the CT state. While other approaches employ an averaging over emission spectra at various geometries, 17,18 our model treats the intermolecular coordinate quantum mechanically, yielding emitting states which themselves are wave function superpositions over Frenkel and CT basis functions with a prescribed number of intermolecular vibrational quanta.

METHODS

In what follows, we consider a simple dimer system, which is useful for understanding excimers in both the solution and crystal phase. In fact, recent studies suggest that in organic thin films the initial delocalized excitation very rapidly localizes to a dimer on a femtosecond time scale, further accentuating the importance of studying dimer systems. However, our model could be straightforwardly extended to a linear stack of three or more chromophores. The model proposed in this paper builds on the physical insight obtained by previous investigations, the first of which corresponds to a structural reorganization of a dimer in the excited state.

The Holstein model includes structural reorganization via a local vibronic coupling term governed by $\hbar\omega\lambda$, where ω is the

vibrational frequency and the dimensionless quantity λ is proportional to the relative displacement between the minima of the ground and excited state potentials along the associated vibrational coordinate (see Figure 1).⁴⁴ The corresponding nuclear relaxation energy is given by $\hbar\omega\lambda^2$, where λ^2 is the Huang–Rhys (HR) factor.

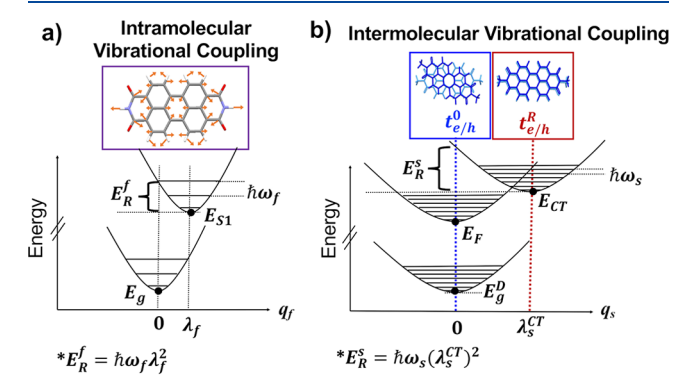


Figure 1. Diabatic potential wells corresponding to (a) the fast intramolecular vibration along coordinate, q_b and (b) the slow intermolecular vibration along coordinate q_s . In (b) strong local coupling of the CT state $(|1^+2^-\rangle \text{ or } |2^+1^-\rangle)$ is represented by a significant shift of the potential well along q_s relative to the ground state well. The intramolecular vibrational mode in (a) is represented by a 1400 cm⁻¹ symmetric vinyl stretching mode. The intermolecular coordinate in (b) includes a change in the relative orientation (angle) between the two PDI molecules in the dimer. The operator form of the dimensionless coordinate, $\hat{q}_s = (b_s^\dagger + b_s)/2$, is consistent with the shift of the CT well minimum by λ_s^{CT} . A similar construct for the coordinate operator applies to the fast mode.

Our previous work on systems of small organic chromophores or polymers has mainly focused on intramolecular vibrational coupling involving a fast vinyl stretching mode $\omega_{\rm f} \approx$ 1400 cm⁻¹ in aromatic systems with a HR factor $\lambda_{\rm f}^{\,2} \approx 1$ obtained from experimental monomer spectra (Figure 1a). 35,36 In the present work, we incorporate structural reorganization along an intermolecular coordinate in the dimer excited state through a slow intermolecular vibrational mode, with the coupling governed by $\hbar\omega_s\lambda_s$. We consider a mode energy of the order of $\omega_s\approx 100~{\rm cm}^{-1}$, an order of magnitude smaller than the intramolecular mode, but with a HR factor as high as 20 in order to obtain a substantial relaxation energy. Such a mode has been deemed essential for excimer formation.⁴⁵ The mode can consist of any compression, sliding or torsional motion; the specifics are not required as input in the proposed model. In the following analysis, it is assumed that the motion is along the coordinate which relaxes to the dimer's first excited state minimum, which is assumed to be a torsional motion in PDI¹³ or perylene¹⁴ dimers.

The inclusion of *inter*molecular vibrations with large reorganization energies has the ability to induce a large Stokes shift and broadening, two typical features of excimer spectral signatures. To this end, one must consider how progression along the intermolecular coordinate impacts the energies of the various dimer excited states (i.e., Frenkel-like vs CT) with the possible formation of new excited state equilibrium geometries, where the reorganization energy relates to the strength of the coupling through λ_s . As pointed out previously, ⁴⁶ the coupling can be significant in excited states with a large CT character, since relative changes in orientation between a cation and anion will influence the site energy of the CT state. Therefore,

we introduce local *inter*molecular vibrational coupling to the CT states, but neglect it for the Frenkel states, as depicted in Figure 1b.

Intermolecular vibrations will not only impact the local diabatic energies as described above but will also induce changes in the electronic coupling between the monomeric components of the dimer during evolution along the intermolecular mode (Figure 1b). While exciton coupling between transition dipoles requires large changes in geometry in order to significantly alter the coupling, it has been previously demonstrated that the transfer integrals involved in Frenkel-CT coupling are highly sensitive to even small sub-Angstrom shifts in relative geometry. 47 Therefore, the so-called nonlocal coupling between Frenkel and CT states induced by the intermolecular mode will be incorporated in our model, while nonlocal coupling between Frenkel states is assumed to be negligible. Many groups have previously included nonlocal intermolecular coupling in dynamics studies either by using a Holstein-Peierls Hamiltonian 48,49 or by Taylor expanding the coupling constants along a Born-Oppenheimer intermolecular vibrational coordinate.

Overall, the Holstein–Peierls (HP) Hamiltonian analyzed in this work can be decomposed into pure electronic components consisting of Frenkel ($H_{\rm F}$) and CT ($H_{\rm CT}$) terms as well as vibrational/vibronic terms involving the fast *intra*molecular mode ($H_{\rm vib}^{\rm f}$) and the slow *inter*molecular mode ($H_{\rm vib}^{\rm f}$),

$$H_{\rm HP} = H_{\rm F} + H_{\rm CT} + H_{\rm vib}^{\rm f} + H_{\rm vib}^{\rm s}$$
 (1)

For a dimer, the electronic Frenkel Hamiltonian can be expressed as

$$H_{\rm F} = E_{\rm S1}[11\rangle\langle 11 + |2\rangle\langle 21] + J_{\rm C}[|1\rangle\langle 21 + |2\rangle\langle 11] \tag{2}$$

where the state $|n\rangle$ (n=1,2) indicates that the nth monomer is electronically excited to the S_1 state, while the remaining monomer is unexcited (S_0). The $S_0 \rightarrow S_1$ transition energy is E_{S1} and J_C is the Coulomb coupling due to interacting HOMO \rightarrow LUMO transition dipole moments on neighboring chromophores. Next, the CT electronic part of the dimer Hamiltonian in eq 1 can be expressed as

$$H_{\text{CT}} = E_{\text{CT}}(|1^{+}, 2^{-}\rangle\langle 1^{+}, 2^{-}| + |2^{+}, 1^{-}\rangle\langle 2^{+}, 1^{-}|)$$

$$+ t_{e}(|1^{+}, 2^{-}\rangle\langle 1| + |2^{+}, 1^{-}\rangle\langle 2| + \text{h.c.})$$

$$+ t_{h}(|1^{+}, 2^{-}\rangle\langle 2| + |2^{+}, 1^{-}\rangle\langle 1| + \text{h.c.})$$
(3)

which includes the CT site energies $E_{\rm CT}$ as well as the coupling between Frenkel and CT states through the electron (hole) dissociation integrals, which under the approximation of a one-electron Hamiltonian (\hat{h}) are equivalent to the electron (hole) transfer integrals $t_{\rm e}(t_{\rm h})$. The electron (hole) transfer integrals are related to the molecular orbital overlap between the LUMO (HOMO) orbitals of the monomers A and B,

$$t_{\rm e} = \langle {\rm LUMO_A} | \hat{h} | {\rm LUMO_B} \rangle$$

$$t_{\rm h} = -t_{\rm H} = -\langle {\rm HOMO_A} | \hat{h} | {\rm HOMO_B} \rangle$$
(4)

The hole transfer integral is negated relative to the matrix element of \hat{h} connecting two neighboring HOMO orbitals $(t_{\rm H})^{.50}$ This arises because moving a hole forward is equivalent to moving a valence electron backward. Generally, the signs of $t_{\rm e}$ and $t_{\rm h}$ depend on the chosen phase convention which relates the molecular orbitals on A to those on B. ⁵¹ The phase

convention must be consistent with the directions of the transition dipole moments on A and B.

Within the electronic basis set, the two diabatic Frenkel states of the dimer are defined as,

$$|k = 0\rangle_{F} = \frac{1}{\sqrt{2}}\{|1\rangle + |2\rangle\}$$

$$|k = \pi\rangle_{F} = \frac{1}{\sqrt{2}}\{|1\rangle - |2\rangle\}$$
(5)

For dimers with aligned transition dipole moments, the phase convention is chosen such that only the k=0 state is optically allowed from the vibrationless electronic ground state. There are also two diabatic symmetry-adapted CT states

$$|k = 0\rangle_{\text{CT}} = \frac{1}{\sqrt{2}} \{|1^{+}, 2^{-}\rangle + |2^{+}, 1^{-}\rangle\}$$

$$|k = \pi\rangle_{\text{CT}} = \frac{1}{\sqrt{2}} \{|1^{+}, 2^{-}\rangle - |2^{+}, 1^{-}\rangle\}$$
(6)

Finally, only states with the same momentum couple, producing two upper (+) and two lower (–) adiabatic eigenstates of the purely electronic Hamiltonian $H_{\rm F}+H_{\rm CT}$:

$$|k\rangle_{F,CT}^{\pm} = c_F^{k,\pm}|k\rangle_F + c_{CT}^{k,\pm}|k\rangle_{CT}$$
(7)

where the relative Frenkel (CT) character of each state is given by its coefficients $c_{\rm F}^{k,\pm}$, $c_{\rm CT}^{k,\pm}$. For a dimer, the kth eigenvalue ($k=0,\pi$) in the upper (+) or lower (-) band is

$$E_{\pm}^{k} = \frac{E_{F}^{k} + E_{CT}}{2}$$

$$\pm \sqrt{\left(\frac{E_{CT} - E_{F}^{k}}{2}\right)^{2} + t_{e}^{2} + t_{h}^{2} + 2t_{e}t_{h}\cos(k)}$$
(8)

where $E_{\rm F}^k = E_{S_1} + J_{\rm C}\cos(k)$. Note that the energy expression in eq 8 slightly differs from that corresponding to a linear aggregate with periodic boundary conditions due to the latter having two nearest neighbors.⁴⁷

The third term in the Hamiltonian in eq 1 accounts for local vibronic coupling involving the fast *intra*molecular mode with frequency ω_f as was done in our previous works. The HR factor for the shifted harmonic well corresponding to state S_1 is λ_f^2 , while the HR factors for the shifted cation and anion wells are $(\lambda_f^+)^2$ and $(\lambda_f^-)^2$, respectively. In the Hamiltonian, $b_n^{\dagger}(b_n)$ is the creation (annihilation) operator of a vibration in the S_0 potential on chromophore n, where we have suppressed the subscript f for notational simplicity. Assuming periodic boundary conditions, the Hamiltonian reads:

$$H_{\text{vib}}^{f} = \omega_{f} b_{n}^{\dagger} b_{n} - \omega_{f} \lambda_{f} \sum_{n=1}^{2} \left[(b_{n}^{\dagger} + b_{n}) - \lambda_{f} \right] |n\rangle \langle n|$$

$$- \omega_{f} \lambda_{f}^{+} \sum_{n=1}^{2} \left[(b_{n}^{\dagger} + b_{n}) - \lambda_{f}^{+} \right]$$

$$\times |n^{+}, (n+1)^{-}\rangle \langle n^{+}, (n+1)^{-}|$$

$$- \omega_{f} \lambda_{f}^{-} \sum_{n=1}^{2} \left[(b_{n+1}^{\dagger} + b_{n+1}) - \lambda_{f}^{-} \right]$$

$$\times |n^{+}, (n+1)^{-}\rangle \langle n^{+}, (n+1)^{-}|$$
(9)

where we have set $\hbar=1$. (Note under periodic boundary conditions chromophore n+1 is understood to be chromophore 1 when n is 2.) In the following analysis, we approximate $(\lambda_{\rm f}^+)^2+(\lambda_{\rm f}^-)^2\approx \lambda_{\rm f}^2$ and $(\lambda_{\rm f}^+)^2=(\lambda_{\rm f}^-)^2$ as done in previous work. 52,53

The final additions to the Holstein–Peierls Hamiltonian, which are essential to excimer formation, incorporate the coupling to an effective slow *inter*molecular vibrational mode, with frequency $\omega_s \approx 100~{\rm cm}^{-1}$. The local $(H_{\rm L}^{\rm s})$ and nonlocal $(H_{\rm NL}^{\rm s})$ components involving only the slow mode are expressed through

$$H_{\text{vib}}^{s} = \omega_{s} b_{s}^{\dagger} b_{s} + H_{\text{L}}^{s} + H_{\text{NL}}^{s} \tag{10}$$

where b_s^{\dagger} (b_s) is the creation (annihilation) operator of an *inter*molecular phonon in the unshifted potential of the dimer. The *local* coupling involving the slow mode is accounted for in H_L^s and represents a shift of the harmonic potential well only for CT states with HR factor ($\lambda_s^{\rm CT}$)². We have,

$$H_{\rm L}^{\rm s} = -\omega_{\rm s} \lambda_{\rm s}^{\rm CT} \sum_{n=1}^{2} \left[(b_{\rm s}^{\dagger} + b_{\rm s}) - \lambda_{\rm s}^{\rm CT} \right] |n^{+}, (n+1)^{-} \rangle \langle n^{+}, (n+1)^{-} |$$
(11)

Additionally, nonlocal coupling involving the slow mode is manifested in potentially large changes in the Frenkel-CT coupling along the *inter*molecular coordinate, q_s , as realized, for example, by the increased molecular orbital overlap in the relaxed excimer geometry. ⁵⁴ We incorporate this effect by expanding $t_{e/h}$ to first order in q_s

$$t_{\rm e/h} \approx t_{\rm e/h}^0 + g_{\rm e/h} q_{\rm s} \tag{12}$$

where $t_{\rm e}^0$ and $t_{\rm h}^0$ represent the electron and hole transfer integrals, respectively, corresponding to the relaxed ground state geometry (see Figure 1), and where the nonlocal coupling is governed by

$$g_{\rm e/h} \equiv \frac{\partial t_{\rm e/h}}{\partial q_{\rm s}}$$
 (13)

One can incorporate the nonlocal coupling term, $g_{\rm e/h}q_{\rm s}$, quantum mechanically through a Holstein–Peierls model. In reduced coordinates, the nonlocal Frenkel-CT coupling term in the Hamiltonian can be written as

$$H_{\rm NL}^{\rm s} = g_{\rm e} \frac{(b_{\rm s}^{\dagger} + b_{\rm s})}{2} (|1^{+}, 2^{-}\rangle\langle 1| + |2^{+}, 1^{-}\rangle\langle 2| + \text{h.c.})$$

$$+ g_{\rm h} \frac{(b_{\rm s}^{\dagger} + b_{\rm s})}{2} (|1^{+}, 2^{-}\rangle\langle 2| + |2^{+}, 1^{-}\rangle\langle 1| + \text{h.c.})$$
(14)

where the operator form of the dimensionless coordinate q_s is $\hat{q}_s = (b_s^\dagger + b_s)/2$. With q_s so defined, its expectation value at the diabatic CT potential minimum occurs when $\langle q_s \rangle = \lambda_s^{\rm CT}$. Hence, the nonlocal coupling parameter can be approximated (assuming $\lambda_s^{\rm CT} \neq 0$) from the extreme geometries as

$$g_{\rm e/h} \approx \frac{t_{\rm e/h}^{\rm R} - t_{\rm e/h}^{\rm 0}}{\lambda_{\rm s}^{\rm CT}} \tag{15}$$

where t_e^R and t_h^R are the electron and hole transfer integrals, respectively, calculated at the relaxed excited state geometry, see Figure 1.

The basis set used in this paper is similar to the multiparticle basis set pioneered by Philpott⁵⁵ and applied in many previous

works involving Frenkel-CT coupling; 35,47,56 however, here we include an additional intermolecular vibrational degree of freedom. Accordingly, one-particle states are represented as $|n, \tilde{\nu}; \nu_s^F\rangle$, where an exciton is localized on site n with $\tilde{\nu}$ intramolecular vibration quanta in the S_1 potential, while the neighboring chromophore is in its electronic ground state, with no vibrational quanta in the S_0 potential. In addition, there are ν_s^F vibrational quanta in the *inter*molecular potential well corresponding to the Frenkel (F) exciton. Two-particle states, I $n, \tilde{\nu}; n', \nu'; \nu_s^F \rangle$, include at least one additional *intra*molecular vibration ν' in the neighboring chromophore's (n') groundstate (S_0) potential. Finally, the charge transfer states can be written as $|n^+, \nu^+; (n+1)^-, \nu^-; \nu_s^{CT}\rangle$, where a cation is localized on site n^+ with an *intra*molecular vibration ν^+ in the cation potential and an anion is localized on the neighboring chromophore $(n + 1)^-$ with an *intra*molecular vibration $\nu^$ in the anion potential. (For a dimer, chomophore n + 1 is understood to be chromophore 1 when n is 2). In addition, there are ν_s^{CT} intermolecular vibrational quanta in the (shifted) harmonic well corresponding to the CT state. It is important to note that the basis set so described is formally complete for a dimer. A given eigenstate of H_{HP} can then be expanded as,

$$\begin{split} |\Psi_{\alpha}\rangle &= \sum_{n,\widetilde{\nu}} \sum_{\nu_{s}^{F}} c_{n,\widetilde{\nu};\nu_{s}^{F}}^{\alpha} |n,\,\widetilde{\nu};\,\nu_{s}^{F}\rangle \\ &+ \sum_{n,\widetilde{\nu}} \sum_{n',\nu'} \sum_{\nu_{s}^{F}} c_{n,\widetilde{\nu};n',\nu';\nu_{s}^{F}}^{\alpha} |n,\,\widetilde{\nu};\,n',\,\nu';\,\nu_{s}^{F}\rangle \\ &+ \sum_{n,\nu^{+},\nu^{-}} \sum_{\nu_{s}^{CT}} c_{n,\nu^{+},\nu^{-};\nu_{s}^{CT}}^{\alpha} |n^{+},\,\nu^{+};\,(n+1)^{-},\,\nu^{-};\,\nu_{s}^{CT}\rangle \end{split}$$

$$\tag{16}$$

Generally, an emitting state of the form eq 16 possesses qualities of both Frenkel and CT excitons, yielding observables which take on an intermediate character. For example, under local coupling, the expectation value of the slow coordinate q_s lies between 0 (Frenkel-exciton) and $\lambda_s^{\rm CT}$ (CT-exciton). This view is consistent with the findings of refs 57 and 58, where vibrational spectroscopy was used to show that in certain molecular dimers, the excimer properties are intermediate between those of local and CT excitations.

Absorption and emission formulas incorporating *inter*molecular vibrations are listed in section SI.2, using the dipole operator defined as

$$\hat{\mu} = \vec{\mu}_{\rm F} \{ |g\rangle\langle 1| + |g\rangle\langle 2| + \text{h.c.} \}$$
 (17)

where |g| represents the electronic ground state. For the absorption spectra, hot transitions are included by taking a thermal average over a Boltzmann distribution of vibrationally excited electronic ground states. A Boltzmann distribution of the emitting eigenstates was also taken to determine the temperature-dependent emission spectra. In what follows, we neglect the effects of self-absorption, disorder, and triplet states, the small CT transition dipole moment, as well as the anharmonicity of low-frequency wells. Furthermore, we assume that the k = 0 exciton retains all of the oscillator strength, and therefore neglect any dipole moment misalignments caused by motion along the intermolecular coordinate. For the bis-PDI-A and bis-PDI-B applications, we therefore neglect the oscillator strength of the lower Davydov component induced by the small deviations from an eclipsed geometry. We found that these approximations do not effect the essential physics of

excimer formation, and the details of their photophysical effects will be left for future work.

RESULTS AND DISCUSSION

Local and Nonlocal Intermolecular Coupling in Linear Absorption Spectra. The model proposed in this work is able to simulate *both* the absorption and emission spectra with a common set of parameters. Figure 2 depicts the

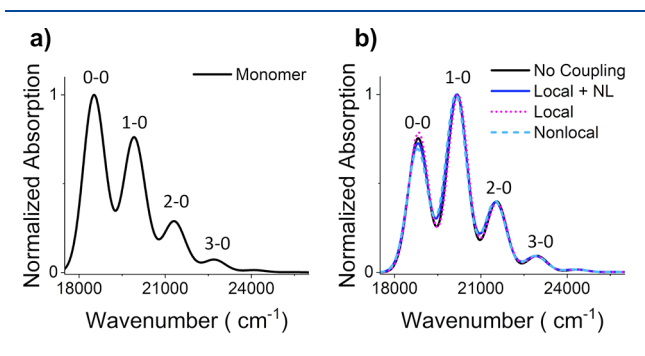


Figure 2. Calculated room temperature linear absorption spectrum of (a) a PDI monomer and (b) an eclipsed ("sandwich") dimer which demonstrates the effect of H-promoting electronic couplings ($J_{\rm C}>0$, $t_{\rm e}t_{\rm h}<0$) in inverting the relative intensities of the first two vibronic peaks, independent of slow-mode coupling. In (b) the full Hamiltonian, $H_{\rm HP}$, is employed. Only small changes are caused by the local $((\lambda_{\rm s}^{\rm CT})^2=14)$ and nonlocal $(g_{\rm h}=-g_{\rm e}=280~{\rm cm}^{-1})$ intermolecular coupling terms in eq 1. Spectra were simulated with the parameters: $E_{\rm CT}-E_{\rm SI}=1400~{\rm cm}^{-1}$, $J_{\rm C}=333~{\rm cm}^{-1}$, $t_{\rm h}=-t_{\rm e}=280~{\rm cm}^{-1}$, $\omega_{\rm s}=100~{\rm cm}^{-1}$, $\omega_{\rm f}=1400~{\rm cm}^{-1}$, $\lambda_{\rm f}^2=0.7$, and with a linewidth of 420 cm⁻¹. For the "No Coupling" curve (black) in (b): $\lambda_{\rm s}^{\rm CT}=g_{\rm e}=g_{\rm h}=0$.

calculated absorption spectrum of a PDI monomer (Figure 2a) and a model HH-dimer (Figure 2b) using the Hamiltonian in eq 1 (see the Supporting Information for details). The clear vibronic progression observed in both the monomer and dimer is a result of local coupling to the fast *intra*molecular mode. In the dimer, the molecules are eclipsed so that the transition dipole moments on each monomer are parallel as in an Haggregate. Accordingly, the Coulomb coupling is positive and the electron and hole transfer integrals out-of-phase (H-like), as is the case for the PDI dimers considered in detail later on. Hence, the dimer can be described as a HH-aggregate. Accordingly, in going from the monomer to the dimer, one observes an inversion of the ratio between the first two vibronic peaks.

Furthermore, Figure 2 demonstrates that, in the case of this study's experimentally relevant couplings, which includes also out-of-phase nonlocal couplings $(g_e = -g_h)$; see section Comparison to Experiment), the absorption spectrum is practically unchanged by the inclusion of either local or nonlocal coupling to the slow, intermolecular mode. This supports the approach in previous works that the coupling parameters corresponding to the ground state geometry are mainly responsible for the absorption spectrum. Hestand and Strong demonstrated how nonlocal couplings can variously broaden the different k exciton states in linear absorption spectra;³⁷ however, in their model, the nonlocal coupling is incorporated indirectly through an average over different ground-state geometries produced by molecular dynamics. Our model is restricted to a single intermolecular mode, but treats the nonlocal (and local) coupling fully quantum mechanically.

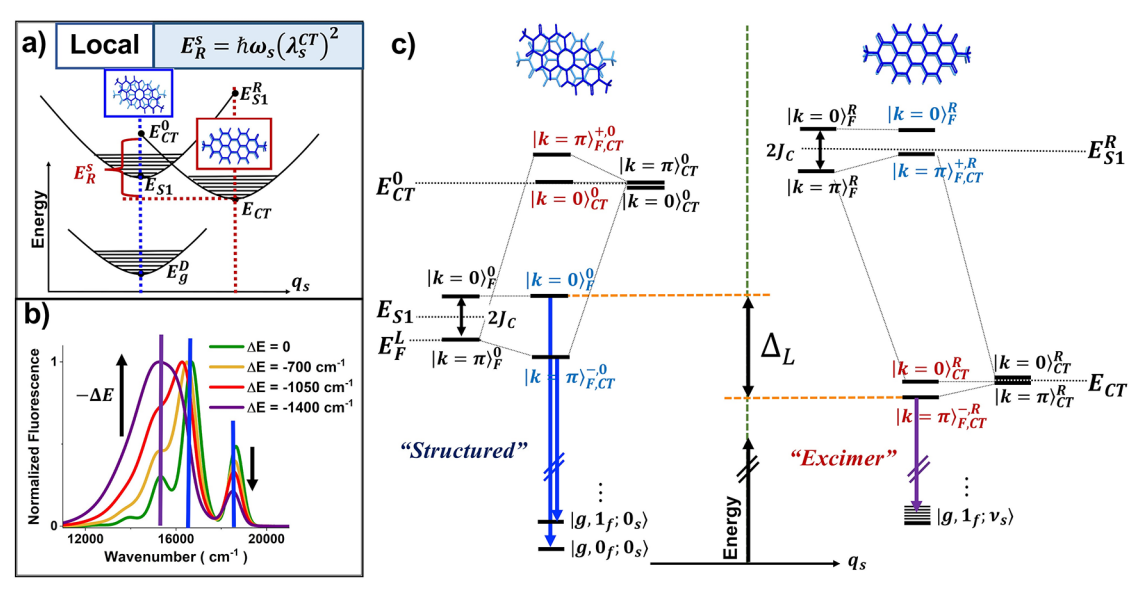


Figure 3. (a) Diabatic potential wells corresponding to local (S_1) and CT excitations in a dimer, drawn with respect to the intermolecular coordinate, q_s . E_{S_t} , E_{CT}^0 correspond to the ground state geometry and E_{CT} , $E_{S_1}^R$ correspond to the relaxed first excited state geometry along q_s . (b) Calculated room temperature fluorescence spectrum based on $H_{HP} - H_{NL}^s$ displaying excimer formation upon stabilizing E_{CT} , where $\Delta E = E_{CT} - E_{S_1}$. Parameters: $J_C = 333$ cm⁻¹, $t_h^0 = -t_e^0 = 420$ cm⁻¹, $\lambda_f^2 = 0.7$, $(\lambda_s^{CT})^2 = 15$, $\omega_s = 100$ cm⁻¹, $\omega_f = 1400$ cm⁻¹, and a line width of 420 cm⁻¹. c) Simplified energy level diagram for the geometry corresponding to the minimum of the Frenkel well (left) and at the minimum of the CT well (right) when $t_h^0 = -t_e^0$. The splitting at the eclipsed geometry (right) is the source of the excimer peak (dark purple) in b) and its large CT character, when $E_{CT} < E_F^1$. The splitting at the ground state geometry (left) is responsible for the thermally activated structured emission deriving from the upper Frenkel-like states (blue), dressed with *intra*molecular vibrations. Δ_L represents the energy difference between the relaxed $k = \pi$ excimer state and the unrelaxed Frenkel-like k = 0 state. Note: this cartoon depicts only the electronic diabatic states where only the *inter*molecular vibrational coordinate is considered. *Intra*molecular vibrations also couple to the transitions as seen in b), and are only included in the electronic ground state to which emission occurs in (c), in order to satisfy symmetry requirements (see text).

Although the absorption spectrum is practically unaffected by either local or nonlocal intermolecular coupling involving the slow mode, such is not the case for the fluorescence spectrum. As demonstrated in the following sections, emission is profoundly impacted by the slow mode, which causes evolution toward a relaxed excited state. Whereas absorption is mainly governed by transitions from the ground state, along with a few hot-band transitions involving the slow intermolecular mode, emission derives from a relaxed (displaced) excited state geometry with transitions terminating on a number of intermolecular vibrational quanta in the electronic ground state potential. As discussed in the proceeding sections, not all coupled Frenkel-CT states are shifted equally along the intermolecular coordinate, making for a rather complex emission profile, generally consisting of structured and unstructured elements.

Excimer Mechanisms. Previous work suggests that excimer emission arises due to Frenkel-CT mixing. 10,59 In a closely-packed π -stacked system, the molecular orbital overlap will induce mixing between Frenkel and CT excitons through eq 4. Prior implementations of a Frenkel-CT Holstein model (based on the first three terms in eq 1) have analyzed absorption and fluorescence spectral signatures of Frenkel-CT interference in closely-packed organic aggregates that display only vibronically structured emission, but no evidence of excimers. 35,56 To describe excimer formation, one requires at least Frenkel-CT mixing and relaxation along a slow mode.

The increase in Frenkel-CT mixing that is induced by the larger π -orbital overlap at a new relaxed geometry is believed to generate excimer signatures in the fluorescence. Several experiments distinguish between CT states and excimer states

by the amount of charge transfer character at the excimer geometry, ^{21,29} where transient absorption excimer signatures typically do not exhibit pure anion and cation peaks. ^{27,60} However, the exact mechanism of excimer formation and a clear role of the CT states or Frenkel-CT mixing in excimer emission are not well understood. The following sections aim to provide further insight into the role that CT states and *inter*molecular vibrations play in inducing excimer emission in molecular dimers.

Excimers via Local CT Coupling to the Intermolecular Mode. The electronic interference between Frenkel and CT excitons in a molecular dimer can be visualized through the following coupling matrix element, which makes use of eqs 3, 5, and 6:

$${}_{F}\langle k|H_{\rm CT}|k\rangle_{\rm CT} = t_{\rm e}^0 + {\rm e}^{ik}t_{\rm h}^0 \tag{18}$$

Hence, when $t_{\rm e}^0=t_{\rm h}^0$ only the optically bright k=0 Frenkel exciton and k=0 CT exciton will mix. Conversely, when $t_{\rm e}^0=-t_{\rm h}^0$, as is relevant in the present work, only the optically dark $k=\pi$ states will mix. In real systems, the transfer integrals are unequal in magnitude and therefore mixing between both the Frenkel and CT k=0 states as well as between both the Frenkel and CT $k=\pi$ states will occur. Nevertheless, one can see that the two optically allowed adiabatic Frenkel-CT k=0 states can have varying degrees of Frenkel and CT character, depending on the signs and magnitudes of the transfer integrals, as well as the energy mismatch between E_F and E_{CT} .

Incorporating local *inter*molecular vibrational coupling to the CT state of the dimer via $H_{\rm L}^{\rm s}$ leads to a shifted CT diabatic well relative to the Frenkel diabatic well, as depicted in Figure 3a. The energetic offset between the diabatic Frenkel and CT

states and hence the Frenkel-CT mixing now evolves along the coordinate q_s , as the CT state is increasingly stabilized and the Frenkel state is increasingly destabilized, leading to greater CT character in the relaxed excited state vs ground state geometries. The electronic coupling will also be modulated by *inter*molecular overlap factors:

$${}_{\mathsf{F}}\langle k; \, \nu_{\mathsf{s}}^{\mathsf{F}} | H_{\mathsf{CT}} | k; \, \nu_{\mathsf{s}}^{\mathsf{CT}} \rangle_{\mathsf{CT}} = \{ t_{\mathsf{e}}^{0} + \mathsf{e}^{ik} t_{\mathsf{h}}^{0} \} \langle \nu_{\mathsf{s}}^{\mathsf{F}} | \nu_{\mathsf{s}}^{\mathsf{CT}} \rangle \tag{19}$$

Under the assumption that $\lambda_s^{\rm CT}$ is large, corresponding to a large reorganization energy of the CT state along an *inter*molecular vibrational coordinate, our model shows that a Stokes shift and broadening can occur in the emission spectrum even without the implementation of the *nonlocal* coupling ($g_e = g_h = 0$), as long as the diabatic CT minimum is sufficiently below that of the lowest electronic Frenkel state (see Figure 3):

$$E_{\rm CT} < E_{\rm F}^{\rm L} \tag{20}$$

In section SI.3, we show through perturbation theory how an *inter*molecular Stokes shift is induced under the inequality (eq 20). With the incorporation of *intra*molecular vibronic coupling, it is possible to obtain excimer formation for both relative phase combinations between $t_{\rm e}^0$ and $t_{\rm h}^0$ via local *inter*molecular vibronic coupling to the CT states; however, here we focus on the experimentally relevant case $t_{\rm e}^0 \approx -t_{\rm h}^0$, as observed in bis-PDI A and B quantum calculations listed in Table 1 in the Comparison to Experiment section. Further investigation into how the different relative phase combinations affects excimer signatures will be left to future work.

Figure 3b shows how the calculated room-temperature emission spectrum for an HH-aggregate varies with increasing CT state stabilization. The spectra are evaluated using H_{HP} – $H_{\rm NL}^{\rm s}$ and therefore include *intra*molecular vibrational coupling in addition to local intermolecular vibrational coupling. When $E_{\rm CT}$ and $E_{\rm S_1}$ are equal, the spectrum contains a pronounced vibronic structure, resembling a progression based on the fast intramolecular mode. However, as E_{CT} dips below E_{S} , the emission becomes more red-shifted and excimer-like. The simplified energy level diagram in Figure 3c approximately accounts for the observed behavior. When the energy ordering obeys eq 20, the lowest-energy (excimer) states such as |k| $\pi\rangle_{F,CT}^{R,-}$ and $|k|=0\rangle_{CT}^{R}$ acquire dominant CT character, and are significantly shifted along the intermolecular coordinate. The resulting emission is Stokes-shifted and broadened, since it is composed of transitions which terminate on the electronic ground state with a range of intermolecular quanta. Interestingly, since the *lowest*-energy excimer state arises from $k = \pi$ mixing (since $t_e^0 = -t_h^0$), low-temperature emission must terminate on states with at least one intramolecular vibrational quantum, as is necessary for H-aggregates, where "0-0" emission is forbidden in the ideal case. For example, k = π excimer emission can terminate on the ground electronic state with one intramolecular vibration delocalized over both molecules such that the molecular vibrations are out-of-phase, i.e. a $q = \pi$ phonon state. In this case, an additional 1400 cm⁻¹ Stokes shift will arise.

Under eq 20, the higher-energy eigenstates of $H_{\rm HP}-H_{\rm NL}^{\rm s}$ such as those that derive from $|k=\pi\rangle_{\rm F,CT}^{0-}$ and $|k=0\rangle_{\rm F}^{0}$ (shaded blue in Figure 3c) are more Frenkel-like in character and therefore do not couple as strongly to the *inter*molecular vibrational modes. Emission from such states is characterized by a prominent *intra*molecular vibronic progression, i.e.

"structured" emission. However, since the high-energy states require thermal activation, the structured emission becomes substantial only when the energy gap $\Delta_{\rm L}$, defined in the figure, is not large compared to $k_{\rm b}T$. In the perturbative limit, one can approximate $\Delta_{\rm L} \approx E_{S_1} - E_{\rm CT}$, and hence, the temperature activation is strongly dependent on the diabatic energy gap; structured emission becomes prominent when the Frenkel-CT coupling is relatively weak and the diabatic energy gap $E_{S_1} - E_{\rm CT}$ is small. If one further increases $\Delta_{\rm L}$, for instance, by further stabilizing $E_{\rm CT}$ as shown in Figure 3b, the fluorescence spectrum becomes less structured and almost purely excimerlike. Moreover, for fixed $\Delta_{\rm L}$, the structured emission grows in with increasing temperature, as demonstrated later on (see Comparison to Experiment section).

While incorporation of local vibronic coupling between the CT state and the slow *inter*molecular mode can successfully simulate excimers (Figure 3b), the parameters needed to reproduce experiment are somewhat questionable. Some groups have argued⁶¹ or observed⁶² $E_{\rm CT} < E_{\rm S_1}$ in excimer/exciplex formation. However, others have maintained that $E_{\rm CT}$ cannot be lower in energy than the lowest Frenkel state in perylene diimide dimers. Studies suggest that when including a polarizable medium the energy of the Frenkel state $E_{\rm F}$ can be even more stabilized than the CT state by the crystal's polarizability, and that even if the CT state is in its most stabilized geometry, it is never observed to be more stable than the lowest Frenkel state.

Even though Figure S3 shows that local coupling involving a slow *inter*molecular vibrational mode can induce a structured/ unstructured composite fluorescence spectrum (resembling bis-PDI B in the Comparison to Experiment section), the transfer integrals $t_{\rm e/h}^0$ needed to produce the composite spectrum do not reflect the large molecular orbital overlap in the excited state geometry, and furthermore, $E_{\rm CT}$ is required to be perhaps nonphysically stabilized below $E_{\rm F}^{\rm L}$. The more traditional approach that $E_{\rm CT} > E_{\rm S_1}$ in PDI dimers, as well as the ability to account for larger CT transfer integrals at the excited state geometry, is achievable if one further includes nonlocal *inter*molecular coupling, as discussed in the following section.

Excimers via Nonlocal Frenkel-CT Coupling. Incorporation of the Frenkel-CT nonlocal intermolecular vibrational coupling allows one to account for changes in the CT transfer integrals which occur during relaxation along the intermolecular coordinate. For example, in bis-PDI A and bis-PDI B (see Figure 8 in Comparison to Experiment section), a large increase in the transfer integrals reflects an increase in the molecular π -orbital overlap as the two PDI molecules rotate toward a more eclipsed arrangement. In order to isolate the nonlocally induced excimer behavior, in this section, we neglect the local intermolecular vibrational coupling and set $\lambda_{\rm S}^{\rm CT}=0$. In this case, $g_{\rm e/h}$ are taken from the general expression given by eq 13.

We guide the readers to Brédas et al.'s⁴⁶ intuitive picture describing how nonlocal coupling induces a reorganization energy in the *adiabatic* states. A similar analysis, conducted here under the simplified conditions $E_{\rm CT} = E_{S_1}$ and $J_{\rm C} = 0$, shows that nonlocal coupling induces changes in the *k*-dependent upper-energy (U) and lower-energy (L) potential wells as shown in Figure 4. The minimum of each well is shifted by $\lambda_{\rm U/L}^k$ and relaxed in energy by $E_{\rm R}^k$ with

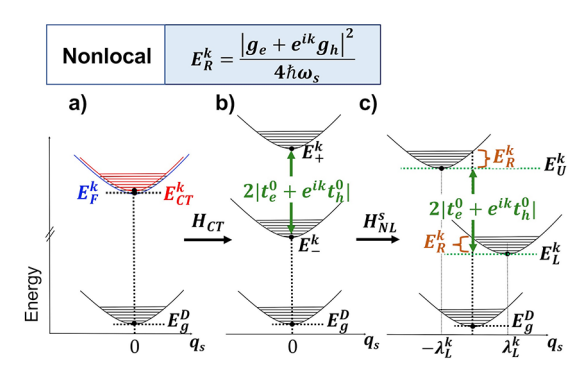


Figure 4. (a) Frenkel and CT diabatic potential wells with respect to the *inter*molecular coordinate under the resonance condition ($E_{\rm CT}=E_{S_1}$) and with $J_{\rm C}=0$. (b) Activating Frenkel-CT mixing via $H_{\rm CT}$ in eq 3 results in split upper (U) and lower (L) Frenkel-CT potential wells, with the well minima given by, E_{\pm}^k from eq 8. (c) Final inclusion of nonlocal coupling via $H_{\rm NL}^s$ results in oppositely displaced potential wells. The well minima are given by $E_{\rm U/L}^k=E_{\pm}^k-E_{\rm R}^k$. Note, the relaxation energy, $E_{\rm R}^k$ is the same for both upper and lower wells.

$$\lambda_{\mathrm{U/L}}^{k} = s_{\mathrm{U/L}}^{k} \frac{g_{\mathrm{e}} + e^{ik} g_{\mathrm{h}}}{2\hbar \omega_{\mathrm{s}}}$$
 (21a)

$$E_{\rm R}^{k} = \frac{|g_{\rm e} + {\rm e}^{ik}g_{\rm h}|^2}{4\hbar\omega_{\rm s}}$$
(21b)

Details of the derivation can be found in SI.6. In eq 21a, $s_{\text{U/L}}^k$ represents a sign, which matches the sign of the product $[-c_h^k \pm c_{\text{CT}}^k]$, with the wave function coefficients taken from eq 7. Hence, for a given k, the upper and lower potential wells are shifted equally, but in opposite directions, as shown in Figure 4. As also indicated in the figure, the relaxation energies, E_R^k (for a given k), are equal for both upper and lower potential wells. Equation 21 highlights how the relative phase between g_e and g_h alters the shifts and reorganization energies of all four potential wells, but the lowest energy well is most relevant for excimer emission. Generally, when the phase relationship between g_e and g_h matches that between t_e^0 and t_h^0 the reorganization energy for the lowest energy state is enhanced, leading to more red-shifted emission.

We now show that nonlocal coupling alone can give rise to a composite emission spectrum. Continuing to adopt this study's experimentally relevant out-of-phase electron and hole transfer integrals, $(t_{\rm h}t_{\rm e}<0)$ as exists in HH-aggregates, Figure 5a, depicts the k-dependence of the upper and lower potential wells when $t_{\rm h}>0$, $t_{\rm e}<0$, and $g_{\rm h}=-g_{\rm e}>0$. With such phase relationships, both $t_{\rm h}$ and $t_{\rm e}$ maintain their phase but increase in magnitude as the molecules progress along the *inter*molecular coordinate. The greatest splitting occurs between the states with $k=\pi$ in accordance with eq 8. Both states have equal relaxation energies, $E_{\rm R}^{\rm m}$, given by eq 21b but with potential wells shifted in opposite directions. By contrast, the k=0 states are entirely unaffected by nonlocal coupling.

Figure 5b demonstrates the evolution of structured-unstructured composite emission spectrum with increasing nonlocal coupling g, where $g=g_{\rm h}~(=-g_{\rm e})$. The calculated spectra are based on the Hamiltonian, $H_{\rm HP}-H_{\rm L}^{\rm s}$ and as such also include intramolecular vibrational coupling. Figure 5b shows how the emission spectrum generally becomes more excimer-like (structureless) with increasing g. Yet, if thermally activated, the unshifted k=0 states can also contribute to the

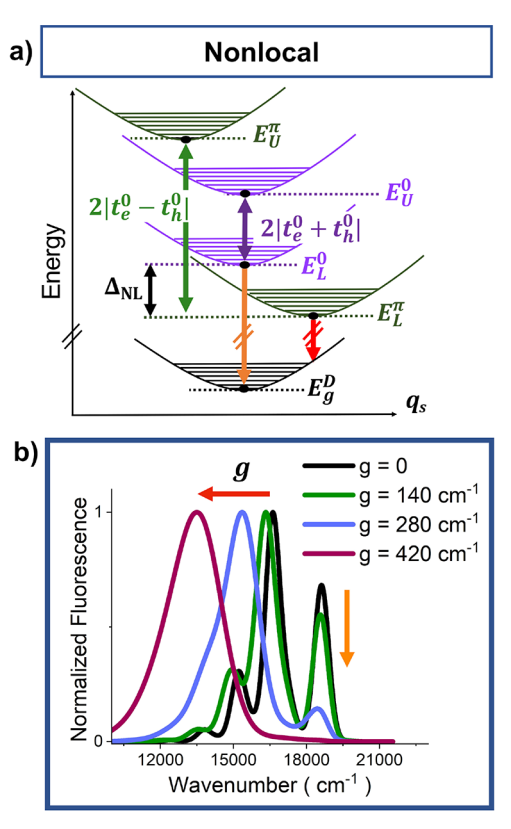


Figure 5. (a) Representation of the four Frenkel-CT adiabats when $g_h = -g_e > 0$, $t_h^0 \approx -t_e^0 > 0$, and $E_{\rm CT} = E_{S_{\rm i}}$. Substantial splitting occurs between the $k = \pi$ states, along with substantial nonlocal shifting and relaxation. By contrast, the k = 0 states are minimally split with no relaxation. Red (orange) arrow represents the excimer (structured) emission. Structured emission from the k = 0 state is thermally activated as $k_{\rm b}T$ approaches $\Delta_{\rm NL}$, with the vibronic structure deriving from intramolecular vibrational coupling. (b) Calculated room temperature fluorescence spectra based on $H_{\rm HP} - H_{\rm L}^{\rm s}$. Note the increasing Stokes shift with increasing $g = g_{\rm h} = -g_{\rm e} > 0$. Here, $E_{\rm CT} = E_{S_{\rm i}}$, $J_{\rm C} = 0$, $t_{\rm h}^0 = -t_{\rm e}^0 = 420$ cm⁻¹, $\omega_{\rm s} = 100$ cm⁻¹, and $\omega_{\rm f} = 1400$ cm⁻¹. In addition, $\lambda_{\rm f}^2 = 0.7$. Note: only the *inter*molecular vibrational coordinate is shown in (a); however, the *intra*molecular vibrations are necessary for $k = \pi$ emission.

fluorescence spectrum, producing an *intra*molecular vibronic progression with a high-energy component near the monomer 0–0 frequency. Figure 5a shows that thermal activation occurs when $k_{\rm b}T$ becomes comparable to or larger than the quantity $\Delta_{\rm NL}$, defined in the figure. Under the simplified conditions in Figure 5, $\Delta_{\rm NL} = |t_{\rm e}^0 - t_{\rm h}^0| - |t_{\rm e}^0 + t_{\rm h}^0| + E_R'(\pi)$. The expression is approximate since it ignores the relatively small changes due to *intra*molecular vibrational coupling.

Unlike for excimer emission induced by local coupling alone, a nonlocally induced Stokes shift and broadening does not require eq 20. Hence, traditional energy orderings for some small organic chromophores such as PDI ($E_{\rm CT} > E_{\rm S_1}$) can be accommodated by the inclusion of nonlocal coupling terms. Figure S4 demonstrates our best attempt to fit the experimental spectrum of bis-PDI B. In order to obtain the correct Stokes shift of the excimer and a more pronounced vibronic progression, we found $E_{\rm CT}$ is required to be much higher than advanced electronic structure methods predict for PDI. While Figures 5a and S4 show how nonlocal intermolecular vibrational coupling can induce excimers in

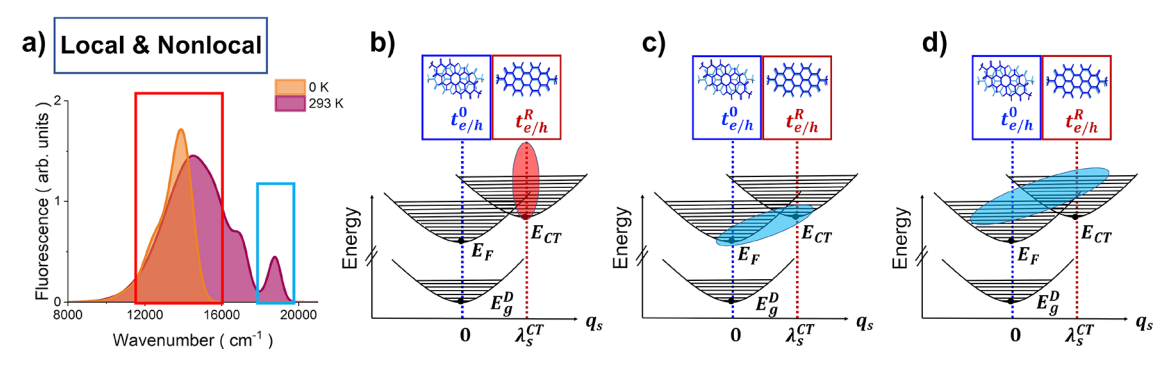


Figure 6. (a) Calculated fluorescence spectrum for an HH-aggregate including local and nonlocal *inter*molecular vibrational coupling at T=0 K (orange) and room temperature (maroon). Here, the complete HP Hamiltonian in eq 1 is employed with $J_{\rm C}=333~{\rm cm}^{-1}$, $t_{\rm h}^0=-t_{\rm e}^0=280~{\rm cm}^{-1}$, $g_{\rm h}=-g_{\rm e}=280~{\rm cm}^{-1}$, $E_{\rm CT}=E_{\rm S_1}=1400~{\rm cm}^{-1}$, $\lambda_{\rm f}^2=0.7$, $(\lambda_{\rm s}^{\rm CT})^2=14$, $\omega_{\rm s}=100~{\rm cm}^{-1}$, $\omega_{\rm f}=1400~{\rm cm}^{-1}$, and a line width of 420 cm⁻¹. (b) Origin of the dominant diabatic couplings responsible for the low-energy excimer emission in (a), where red shading emphasizes the coupling between Frenkel and CT states near the CT minimum geometry. (c) Lower-temperature and (d) higher temperature origins of the dominant diabatic couplings responsible for the high-energy "0–0" emission in (a).

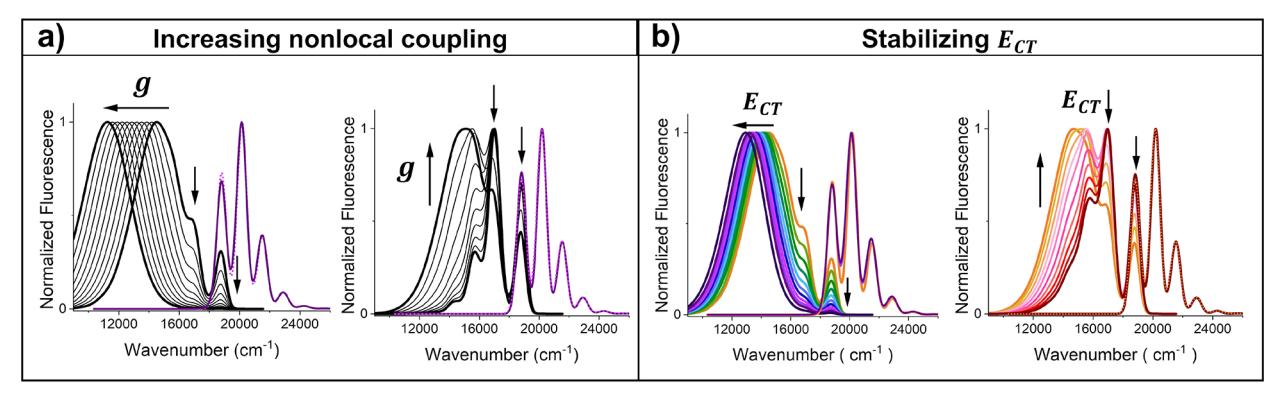


Figure 7. (a) Calculated room temperature absorption and fluorescence spectra for an HH-aggregate based on the HP Hamiltonian in eq 1, demonstrating that the excimer peak grows in with nonlocal coupling, $g = g_h = -g_e > 0$. g increases from 0 to 280 cm⁻¹ in the right panel and continues from 294 to 420 cm⁻¹ in the left panel in increments of 14 cm⁻¹. (b) Calculated room temperature absorption and fluorescence spectra demonstrating excimer formation upon stabilizing $E_{\rm CT}$. $\Delta E = E_{\rm CT} - E_{S_1}$ decreases from 2800 cm⁻¹ (dark red) to 1400 cm⁻¹ in the right panel and continues from 1260 to 140 cm⁻¹ in the left panel, in decrements of 140 cm⁻¹. Absorption spectra are negligibly changed upon increasing g or stabilizing $E_{\rm CT}$. Simulation parameters: $J_{\rm C} = 333$ cm⁻¹, $t_h^0 = -t_e^0 = 280$ cm⁻¹, $\omega_s = 100$ cm⁻¹, $\omega_f = 1400$ cm⁻¹, $\lambda_f^2 = 0.7$, $(\lambda_s^{\rm CT})^2 = 14$, and with a line width of 420 cm, $t_s^{\rm CT} = t_s^{\rm CT$

the fluorescence spectrum, including a higher energy "monomer"-like peak, alone it fails to simulate the experimental spectrum for bis-PDI B with reasonable parameters (Table S3).

Excimers via Local and Nonlocal Coupling. The more realistically "complete" picture, where excimers are formed via both local and nonlocal coupling, is necessary to accurately reproduce experiment with reasonable parameters. With the additional relaxation associated with nonlocal coupling, one can maintain a relatively high energy CT state, which is physically more relevant, and still obtain excimer emission. This is demonstrated in Figure 6a which shows the fluorescence spectrum for a HH-aggregate ($J_{\rm C} > 0$, $t_{\rm e} = -t_{\rm h}$) at T = 0 K and T = 293 K evaluated using the full HP Hamiltonian and with $E_{\rm CT}-E_{\rm S_1}=+1400~{\rm cm}^{-1}$. Based on the coupling parameters in the figure, we obtain $E_{\rm CT}-E_{\rm F}^\pi\approx 1733$ cm⁻¹, in violation of eq 20. In Tables S4-S6, we have analyzed the composition of the emitting eigenstates at both temperatures in order to provide some physical insight into their origin. Figure 6b-d portrays the dominant couplings involved in states providing the excimer-like emission at 0 K (Figure 6b) and the high-energy structured emission at 0K (Figure 6c) and

T=293~K (Figure 6d). It is important to recognize that the eigenstates of the Hamiltonian in eq 1 reflect a quantum mechanical treatment of the nonlocal coupling involving the *inter*molecular coordinate. Accordingly, the total emission spectrum is not simply the average over the q_s -dependent emission spectra, as would be the case if the *inter*molecular coordinate was treated classically via MD simulations.

The low-temperature excimer emission in Figure 6a is due to enhanced relaxation near the CT well minimum $(q_s^0 = \lambda_s^{CT})$ induced by nonlocal coupling. Strong nonlocal coupling arises mainly from the experimentally motivated phases of t_e^0 , t_h^0 , g_{ev} and g_h used in Figure 6, which lead to increases in both $|t_e|$ and lth as one progresses along the intermolecular coordinate toward $q_s^0 = \bar{\lambda}_s^{\text{CT}}$, (see eq 12). When $|g_e|$ and $|g_h|$ are sufficiently large, the resulting Frenkel-CT splitting at $q_s^0 = \lambda_s^{CT}$ is more than enough to drive the energy of the $(k = \pi)$ excimer state low enough to compensate for the energy increase, $E_{\rm CT}-E_{\rm F}$; see Figure 6b. Figure 7a shows that at room temperature the nonlocal coupling g needs to exceed roughly 200 cm⁻¹ in order to achieve dominant excimer emission. In the adiabatic limit, the enhanced relaxation can be understood from Figure 5. The shift of the lowest-energy potential well-induced by the nonlocal coupling is positive (to the right in Figure 5) and

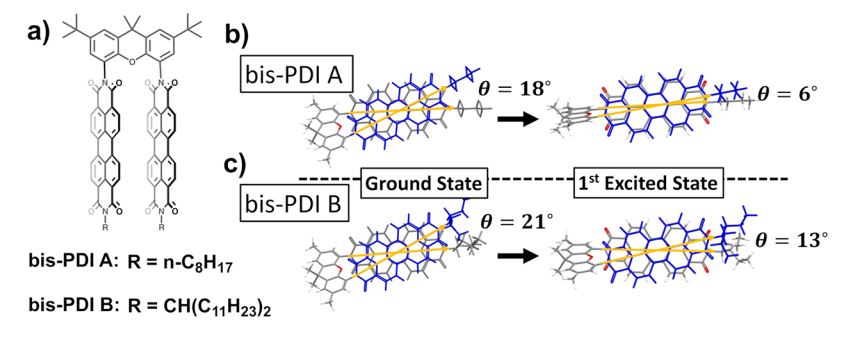


Figure 8. (a) Chemical structure of bis-PDI A and bis-PDI B. Gas phase optimized (b) DFT (TDDFT) ground state (first excited state) geometry of bis-PDI A with truncated $R = C_4H_9$ and (c) TDFT (TDDFT) ground state (first excited state) geometry of bis-PDI B with truncated $R = CH(C_3H_7)_2$, optimized using ω -B97XD/def2-svp in Gaussian 16.

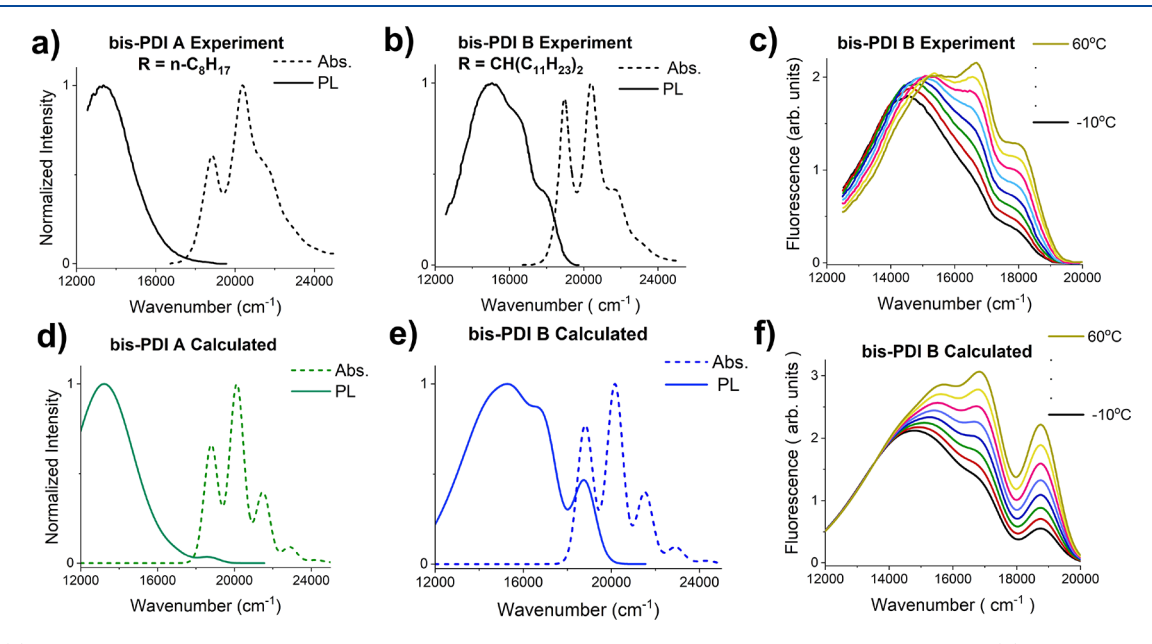


Figure 9. (a) Experimental absorption and emission spectrum of bis-PDI A measured in toluene at room temperature. (b) Experimental absorption and emission spectrum of bis-PDI B measured in toluene at room temperature. (c) Experimental temperature-dependent fluorescence spectra of bis-PDI B from -10 to 60 °C in toluene. (d) Calculated room temperature absorption and emission spectra of bis-PDI A. (e) Calculated room temperature absorption and emission spectra of bis-PDI B. (f) Calculated temperature dependent spectra from -10 to 60 °C. Experimental fluorescence data was digitized from ref 41 and converted to wavenumbers (cm⁻¹) using the appropriate Jacobian factor.⁷⁴ Experimental absorption data was digitized from ref 31 such that toluene is the consistent solvent. Calculated spectra are based on the complete HP Hamiltonian in eq 1 using the fit parameters listed in Table 1.

therefore in the same direction as the shift of the CT minimum $(\lambda_s^{CT} > 0)$, resulting in a constructively enhanced shift and relaxation energy. We will further explore this interesting interference effect in a future work.

The coupling between states with the strongest nonlocal interactions (near $q_s^0 = \lambda_s^{CT}$) is mainly responsible for forming the $k=\pi$ excimer states. Under the parameters considered in Figure 6, the excimer states adopt dominant CT character since at $q_s^0 = \lambda_s^{CT}$ the diabatic CT energy is still lower than the diabatic Frenkel energy (see Figure 6b). The resulting emission at T=0 K is substantially Stokes-shifted (red box Figure 6a), resembling the mechanism of excimer formation through local *inter*molecular coupling alone. Further analysis shows that excimer emission can exist even when the energy of the diabatic CT state is higher than the diabatic Frenkel state near $q_s = \lambda_s^{CT}$, as long as nonlocal coupling is sufficiently strong. Future investigations will consider such excimers with smaller CT character.

In contrast, the structured emission observed at higher temperatures derives from thermally activated states which form from the coupling between low-energy Frenkel-like states and low-energy CT states (see Figure 6c,d), which are weakened by small *inter*molecular vibronic overlap factors. The resulting eigenstates have dominant (k=0) Frenkel exciton character and are responsible for the negligibly Stokes shifted "0–0" emission peak (light blue box Figure 6a), which grows in with temperature. Tables S4–S6 provide more characteristics of all the emitting states, for example their CT character and average shift along the *inter*molecular coordinate.

Since all emitting states derive their oscillator strength from the k=0 Frenkel component, higher-energy states with dominant Frenkel character (and smaller *inter*molecular local and nonlocal coupling), as shown in Figure 6, require only a small population to be observed in the fluorescence spectrum. These higher-energy states become more difficult to temperature-activate if the excimer state is relatively further stabilized. As displayed in Figure 7 this can occur by either (a) increasing

the nonlocal coupling or (b) further stabilizing $E_{\rm CT}$ relative to the monomer transition frequency. One observes from Figure 7 similar trends as seen in the isolated mechanisms due to the (a) nonlocal and (b) local *inter*molecular vibrational coupling.

Interestingly, in the limit of $E_{\rm CT}\gg E_{\rm S_I}$, both the local and nonlocal *inter*molecular coupling appear to have a negligible effect on the fluorescence spectrum (see SI.7) and previous exciton model approaches, which incorporate only the *intra*molecular vibronic coupling to the fast mode ω_{θ} are justified.

Comparison to Experiment. In this section, we apply our model to account for the absorption and emission spectra of two covalently linked dimers of perylene-3,4:9,10-bis-(dicarboximide) derivatives referred to as bis-PDI A and bis-PDI B in Figure 8. In addition, we investigate the temperature-dependent trends for bis-PDI B. Unfortunately, we are not aware of any temperature-dependent spectral recordings for bis-PDI A, to which to compare our theory. Figure 9 displays the experimental absorption and emission spectra, digitized from refs 31 and 41. The figure also shows our simulations based on reasonable physical parameters. Notwithstanding the relative simplicity of the model described herein, it manages to accurately describe the experimental spectra.

Methods and Parameters. Ground state and excited state geometries of the bis-PDIs in Figure 8 were optimized in Gaussian 16^{66} using the ω -B97XD functional⁶⁷ with the def2svp basis set⁶⁸ for DFT and TD-DFT methods, respectively. The functional includes dispersion and has been previously applied to PDI dimers.⁶⁹ The exciton coupling (J_c) and the CT transfer integrals $(t_{e/h}^{0/R})$ were calculated at each geometry. The exciton coupling was calculated using the transition density method, ⁷⁰ and screened by a dielectric constant ($\epsilon = 3$) to account for the solvent environment. The exciton coupling used in the model corresponds to the coupling at the ground state geometry. Nonlocal perturbations to I_C were neglected, as the screened couplings change only from 342 to 393 cm⁻¹ in bis-PDI A and from 327 to 375 cm⁻¹ in bis-PDI B in going from the ground to the first excited state geometries. Transfer integrals were calculated using B3LYP⁷¹ and cc-pVDZ,⁷² where magnitudes and phases were determined through a procedure described in Valeev et al.73 and where the phase convention remains consistent with translational symmetry between monomer orbitals within the dimer.

Table 1 lists parameters from the corresponding quantum mechanical methods calculated for a bis-PDI A and bis-PDI B from Figure 8 with truncated substituents as well as parameters optimized to fit experiment. A monomer frequency of $E_{S_1} = 18\,740~{\rm cm}^{-1}$, an effective *intra*molecular Huang—Rhys factor of 0.7, and an effective *intra*molecular vibrational frequency of 1400 cm⁻¹ were fit to the monomer emission spectrum recorded in ref 41 as shown in Figure S2. The calculated fluorescence spectra do not display any additional spectral shifts outside of what is produced from the given set of parameters. We did, however, add a small gas-to-crystal red shift of about 250 cm⁻¹ to the absorption spectrum of bis-PDI A and bis-PDI B.

The nonlocal couplings listed in Table 1 were calculated from eq 15 using the fit transfer integrals and $\lambda_s^{\rm CT}$. The transfer integrals $t_{\rm e/h}^{\rm O/R}$ needed to fit experiment are smaller than those calculated. However, calculations were performed in the gas phase, neglecting solvation effects. Regardless of the discrepancies in the transfer integrals, the relative trend of increasing

Table 1. Calculated and Optimized Parameters for Bis-PDI A and Bis-PDI B^a

	bis-PDI A		bis-PDI B	
	QC	fit	QC	fit
$E_{CT} - E_{S_1} \text{ (cm}^{-1}\text{)}$		770		770
$t_{\rm e}^0 \ ({\rm cm}^{-1})$	-575	-460	-440	-350
$t_{\mathrm{h}}^{0}~(\mathrm{cm}^{-1})$	444	355	208	166
$t_{\rm e}^{\rm R}~({\rm cm}^{-1})$	-2600	-1490	-1733	-1185
$t_{\rm h}^{\rm R}~({\rm cm}^{-1})$	2240	1741	1946	1250
$g_{\rm e}~({\rm cm}^{-1})$		-230		-187
$g_{\rm h}~({\rm cm}^{-1})$		310		252
$J_{\rm C}~({\rm cm}^{-1})$	342	342	327	327
ϵ		3		3
$\gamma_{\rm em}~({\rm cm}^{-1})$		700		700
$\gamma_{ab} (cm^{-1})$		490		490
$\lambda_{ m f}^{2}$		0.7		0.7
$(\lambda_{ m s}^{ m CT})^2$		20		20
$\omega_{\rm s}~({\rm cm}^{-1})$		100		100
$\omega_{\mathrm{f}}~(\mathrm{cm}^{-1})$		1400		1400

^aDefinitions of parameters are given in the Methods Section of this paper, with the exception of $\sqrt{2\gamma_{\rm em/ab}}$ which defines the standard deviation of the Gaussian line width for the emission/absorption transitions. Note that $J_{\rm C}$ includes screening by the dielectric constant ϵ .

 $t_{\rm c/h}^{0/R}$ in bis-PDI A in both the ground and excited states relative to bis-PDI B holds, which is justified by the changes in orbital overlap due to the steric differences in their substituents. The truly adjustable parameters in our model are mainly $\lambda_{\rm s}^{\rm CT}$ and $E_{\rm CT}-E_{\rm S_1}$. We fixed $E_{\rm CT}-E_{\rm S_1}$ to a value within agreement with previous calculated estimates obtained for PDI, 75 and $\lambda_{\rm s}^{\rm CT}$ was adjusted to fit the experimentally observed Stokes shift and relative composite structured-unstructured emission observed in bis-PDI B. Only electronic coupling parameters were changed in going from bis-PDI B to bis-PDI A. In reality, bis-PDI A's different geometry would induce a different $E_{\rm CT}$ as well as the reorganization energy for the *inter*molecular mode; however, it is assumed these changes are small in order to highlight the trends involving changes in the Frenkel-CT electronic and nonlocal couplings.

Absorption. The absorption spectrum for bis-PDI A and bis-PDI B was also reproduced using the fit parameters listed in Table 1, as shown in Figure 9d,e. The simulated spectrum in each case captures the intensity ratio 0-0/1-0, which is significantly reduced from the monomer ratio (see Figure S2) in both cases. Comparing the vibronic ratios of bis-PDI A and bis-PDI B with that of the monomer, reveals that bis-PDI A is a stronger HH-aggregate 47,51 than bis-PDI B. While both dimers share similar-in-magnitude H-like Coulomb coupling, bis-PDI A has stronger CT-mediated H-like behavior due to larger out-of-phase transfer integrals $t_{\rm e/h}^0$. Thus, the 0-0/1-0 ratio in the spectrum of bis-PDI A is smaller than that observed in bis-PDI B

Structured to Unstructured Excimer Emission. Using the same set of parameters used to simulate the absorption spectra, the model is able to capture discrepancies in the emission spectra between bis-PDI A and B. Interestingly, we find that smaller nonlocal coupling, as for bis-PDI B (in Figure 9b,e), leads to a composite excimer emission spectrum: one that displays both vibronically structured (1400 cm⁻¹ mode) emission as well as unstructured emission. Previously, the structured portion was attributed to monomer contamination.

Conversely, stronger nonlocal coupling, as for bis-PDI A (in Figure 9a,d), leads to a further Stokes-shifted, structureless, more traditional excimer emission.

While the previous Sections imply that conventional excimer emission can arise from a stabilization of the CT state, it is more physically justifiable that excimer emission in bis-PDI A is due to an increase in the nonlocal coupling. This arises from an increase in molecular orbital overlap in the first excited state geometry of bis-PDI A as compared to bis-PDI B (Figure 8). This is not a new concept; previously, Yoo et al. proposed larger orbital overlap in the solid-phase vs solution-phase of PBI B, observing differences in fluorescence intensity and lifetimes between the two phases and hypothesizing that the rigid solid-phase structure favors orbital overlap.⁷⁶ Other previous work has demonstrated that varying the PDI linker can also result in different overlap between dimers and therefore different excimer spectra. 40 However, the connection to the nonlocal intermolecular vibrational coupling was not as clear, nor was there an obvious trend between the amount of orbital overlap in the excited state and spectral features observed in the emission.

The results of bis-PDI B displayed in Figure 9e,f support a mechanism in which the upper k = 0 Frenkel-dominated states are activated with temperature, so that the intramolecular vibronic progression belonging to the Frenkel exciton grows in with temperature. The intramolecular vibronic structure is resolvable because the Frenkel component does not locally couple to intermolecular vibrations. In contrast, in the case of bis-PDI A in Figure 9d, the nonlocal coupling is just large enough for the excimer state(s) to be sufficiently stabilized preventing thermal activation of the states responsible for the vibronically structured emission. It is quite interesting that the unstructured (excimer) emission in bis-PDI B also increases with increasing temperature, as was also found for other covalently linked PDI dimers in ref.²⁸ Our simulations in Figure 9f capture this effect as well. The increase in excimer emission can be traced back to the presence of slightly higher lying k = 0 excimer-like states with higher oscillator strengths than the lowest-lying $k = \pi$ excimer. The observed increase of both components with temperature provides further evidence that the structured emission is not derived from a monomer, or strongly localized dimer state, in equilibrium with the excimer state, since in this case increasing temperature would favor one state at the expense of the other.

While the basic temperature dependence is well-reproduced, the authors acknowledge a discrepancy in the highest energy transition peak in the emission spectrum of bis-PDI B compared to that in experiment. In part, this could be due to the simplicity of our model. However, it is also likely that our DFT/TDDFT calculations cannot accurately reproduce the structure of the dimer in solution. Since the transfer integrals (and therefore the nonlocal couplings) are very sensitive to small shifts in relative geometry, small changes in the dimer's geometry could influence the spectrum. The authors draw attention to the emergence of a higher-energy transition, similar to that which we obtained in our calculations, for bis-PDI B in a different solvent (2-ME-THF).³¹ Figure 9 compares our simulations to experiments done in toluene because this is the solvent at which the temperature-dependence was experimentally recorded. However, overall the basic spectral trends strongly agree with the proposed mechanisms in this paper.

CONCLUSION

The Holstein—Peierls exciton model presented here treats excitons, charge transfer states, *intra*molecular vibrations, and *inter*molecular vibrations all on equal footing. The HP model was shown to capture the basic photophysics of excimer formation in a set of two different covalently linked bis-PDI dimer complexes. Insight from this model suggests that excimer emission can be induced through both local and nonlocal electron-vibrational coupling with respect to a slow *inter*molecular vibrational coordinate, but both mechanisms are required to reasonably simulate experiment.

The model is supported by good agreement with the experimental fluorescence (and absorption) spectra of two different bis-PDI dyes that display different excimer signatures. The out-of-phase electron and hole transfer integrals, $t_e^0 t_h^0 < 0$, in the ground state geometry of the covalently bound dimer reinforce H-like behavior, as reflected in the reduced 0-0/1-0vibronic ratio in the absorption spectrum. Nonlocal coupling derives from the increasing magnitudes of both $t_{\rm e}$ and $t_{\rm h}$ as the molecules progress along the slow coordinate, bringing them into a more eclipsed ("relaxed") geometry where the CT integrals are significantly larger, $|t_e^R| > |t_e^0|$ and $|t_h^R| > |t_h^0|$. We find that the bis-PDI-B complex has smaller nonlocal coupling than bis-PDI-A resulting in the former exhibiting a composite structured/unstructured emission spectrum, whereas bis-PDI-A exhibits the more traditional broad, structureless and redshifted excimer spectrum. The smaller nonlocal coupling in bis-PDI-B is likely due to a large steric hindrance induced by substituents that disfavor molecular orbital overlap in the excited state geometry.

According to our model, the structured features of excimer emission can be attributed to higher-energy states that have dominant Frenkel exciton character which negligibly couple to intermolecular vibrations, but with much stronger coupling to intramolecular vibrations. Hence, the model does not require the presence of monomers to observe structured "monomer"like emission. As demonstrated in the emission spectrum for bis-PDI B, these upper-lying Frenkel-like states are thermally populated so that vibronic structure grows in with increasing temperature. Larger nonlocal Frenkel-CT coupling or further stabilization of the diabatic CT state will induce a larger splitting between the lowest-energy excimer-like state and the Frenkel-like states, resulting in a more traditional broad, structureless, and red-shifted excimer emission. However, under certain conditions, CT state stabilization, achievable, for example, in polar solvents, can lead to symmetry-breaking charge separation (SBCS) which competes with excimer formation, as has been established by several groups for covalently bound PDI dimer complexes. 77-80 Interestingly, SBCS has also been observed in nonpolar solvents, 81 showing that the competition between excimer and SBCS formation is not simply regulated by CT stabilization. We are currently employing our model to further investigate SBCS as well as additional excimer signatures like mid-IR absorption. 82,83

ASSOCIATED CONTENT

Supporting Information

The Supporting Information is available free of charge at https://pubs.acs.org/doi/10.1021/acs.jpcc.1c10255.

Additional calculation details, including experimental monomer spectra, absorption and photoluminescence

equations, derivations, additional calculated spectra, and composition tables regarding the excimer states (PDF)

AUTHOR INFORMATION

Corresponding Author

Frank C. Spano — Department of Chemistry, Temple University, Philadelphia, Pennsylvania 19122, United States; orcid.org/0000-0003-3044-6727; Phone: +1 (215) 204-5203; Email: spano@temple.edu

Author

April L. Bialas – Department of Chemistry, Temple University, Philadelphia, Pennsylvania 19122, United States

Complete contact information is available at: https://pubs.acs.org/10.1021/acs.jpcc.1c10255

Notes

The authors declare no competing financial interest.

ACKNOWLEDGMENTS

This work was performed under the financial support for F.C.S. from the National Science Foundation (DMR-1810838). This research includes calculations carried out on HPC resources supported in part by the National Science Foundation through major research instrumentation Grant Number 1625061 and by the U.S. Army Research Laboratory under Contract Number W911NF-16-2-0189. The authors thank Bernd Engels and David Bialas for engaging and fruitful discussions that helped inspire more in-depth development of this work.

REFERENCES

- (1) Förster, T.; Kasper, K. Ein Konzentrationsumschlag der Fluoreszenz des Pyrens. Z. Elektrochem. 1955, 59, 976–980.
- (2) Birks, J. B.; Christophorou, L. G. Excimer fluorescence spectra of pyrene derivatives. *Spectrochim. Acta* **1963**, *19*, 401–410.
- (3) Birks, J. B.; Dyson, D.; Munro, I. 'Excimer' fluorescence II. Lifetime studies of pyrene solutions. *Proc. R. Soc. London. Ser. A. Math. Phys. Sci.* 1963, 275, 575–588.
- (4) Birks, J. B.; Lumb, M.; Munro, I.; Flowers, B. H. 'Excimer' fluorescence V. Influence of solvent viscosity and temperature. *Proc. R. Soc. London. Ser. A. Math. Phys. Sci.* **1964**, 280, 289–297.
- (5) Birks, J. B.; Christophorou, L. G. Excimer' fluorescence. IV. Solution spectra of polycyclic hydrocarbons. *Proc. R. Soc. London. Ser. A. Math. Phys. Sci.* 1964, 277, 571–582.
- (6) Chandross, E. A.; Ferguson, J. Absorption and Excimer Fluorescence Spectra of Sandwich Dimers of Substituted Anthracenes. *J. Chem. Phys.* **1966**, *45*, 3554–3564.
- (7) Gierschner, J.; Shi, J.; Milián-Medina, B.; Roca-Sanjuán, D.; Varghese, S.; Park, S. Luminescence in Crystalline Organic Materials: From Molecules to Molecular Solids. *Adv. Opt. Mater.* **2021**, 9, 2002251.
- (8) Stevens, B.; Hutton, E. Radiative Life-time of the Pyrene Dimer and the Possible Role of Excited Dimers in Energy Transfer Processes. *Nature* **1960**, *186*, 1045–1046.
- (9) Chen, Z.; Stepanenko, V.; Dehm, V.; Prins, P.; Siebbeles, L. D. A.; Seibt, J.; Marquetand, P.; Engel, V.; Würthner, F. Photoluminescence and Conductivity of Self-Assembled π - π Stacks of Perylene Bisimide Dyes. *Chem. A Eur. J.* **2007**, *13*, 436–449.
- (10) Förster, T. Excimers. Angew. Chemie Int. Ed. 1969, B5, 333-343.
- (11) Pensack, R. D.; Ashmore, R. J.; Paoletta, A. L.; Scholes, G. D. The Nature of Excimer Formation in Crystalline Pyrene Nanoparticles. *J. Phys. Chem. C* **2018**, *122*, 21004–21017.

- (12) Warshel, A.; Huler, E. Theoretical evaluation of potential surfaces, equilibrium geometries and vibronic transition intensities of excimers: the pyrene crystal excimer. *Chem. Phys.* **1974**, *6*, 463–468.
- (13) Fink, R. F.; Seibt, J.; Engel, V.; Renz, M.; Kaupp, M.; Lochbrunner, S.; Zhao, H. M.; Pfister, J.; Würthner, F.; Engels, B. Exciton trapping in π -conjugated materials: A quantum-chemistry-based protocol applied to perylene bisimide dye aggregates. *J. Am. Chem. Soc.* **2008**, *130*, 12858–12859.
- (14) Cook, R. E.; Phelan, B. T.; Kamire, R. J.; Majewski, M. B.; Young, R. M.; Wasielewski, M. R. Excimer Formation and Symmetry-Breaking Charge Transfer in Cofacial Perylene Dimers. *J. Phys. Chem. A* **2017**, *121*, 1607–1615.
- (15) Walker, B.; Port, H.; Wolf, H. The two-step excimer formation in perylene crystals. *Chem. Phys.* **1985**, *92*, 177–185.
- (16) Sung, J.; Kim, P.; Fimmel, B.; Würthner, F.; Kim, D. Direct observation of ultrafast coherent exciton dynamics in helical π -stacks of self-assembled pervlene bisimides. *Nat. Commun.* **2015**, *6*, 8646.
- (17) Gao, F.; Zhao, Y.; Liang, W. Vibronic Spectra of Perylene Bisimide Oligomers: Effects of Intermolecular Charge-Transfer Excitation and Conformational Flexibility. *J. Phys. Chem. B* **2011**, 115, 2699–2708.
- (18) Casanova, D. Theoretical investigations of the perylene electronic structure: Monomer, dimers, and excimers. *Int. J. Quantum Chem.* **2015**, *115*, 442–452.
- (19) Ferguson, J. Absorption and Fluorescence Spectra of Crystalline Pyrene. *J. Chem. Phys.* **1958**, 28, 765–768.
- (20) Azumi, T.; Armstrong, A. T.; McGlynn, S. P. Energy of Excimer Luminescence. II. Configuration Interaction between Molecular Exciton States and Charge Resonance States. *J. Chem. Phys.* **1964**, 41, 3839–3852.
- (21) Ramirez, C. E.; Chen, S.; Powers-Riggs, N. E.; Schlesinger, I.; Young, R. M.; Wasielewski, M. R. Symmetry-Breaking Charge Separation in the Solid State: Tetra(phenoxy)perylenediimide Polycrystalline Films. *J. Am. Chem. Soc.* **2020**, *142*, 18243–18250.
- (22) Kalinowski, J. Excimers and exciplexes in organic electroluminescence. *Mater. Sci.* **2009**, 27, 735–756.
- (23) Bae, Y. J.; Shimizu, D.; Schultz, J. D.; Kang, G.; Zhou, J.; Schatz, G. C.; Osuka, A.; Wasielewski, M. R. Balancing Charge Transfer and Frenkel Exciton Coupling Leads to Excimer Formation in Molecular Dimers: Implications for Singlet Fission. *J. Phys. Chem. A* **2020**, *124*, 8478–8487.
- (24) Chang, X.; Fan, J.; Wang, M.; Wang, Z.; Peng, H.; He, G.; Fang, Y. Dynamic Covalent Chemistry-based Sensing: Pyrenyl Derivatives of Phenylboronic Acid for Saccharide and Formaldehyde. *Sci. Rep.* **2016**, *6*, 31187.
- (25) Traeger, H.; Sagara, Y.; Kiebala, D. J.; Schrettl, S.; Weder, C. Folded Perylene Diimide Loops as Mechanoresponsive Motifs. *Angew. Chem.* **2021**, *60*, 16191–16199.
- (26) Zhang, G.; Yang, G.; Wang, S.; Chen, Q.; Ma, J. S. A Highly Fluorescent Anthracene-Containing Hybrid Material Exhibiting Tunable Blue-Green Emission Based on the Formation of an Unusual "T-Shaped" Excimer. *Chem. A Eur. J.* **2007**, *13*, 3630–3635.
- (27) Sung, J.; Nowak-Król, A.; Schlosser, F.; Fimmel, B.; Kim, W.; Kim, D.; Würthner, F. Direct Observation of Excimer-Mediated Intramolecular Electron Transfer in a Cofacially-Stacked Perylene Bisimide Pair. J. Am. Chem. Soc. 2016, 138, 9029–9032.
- (28) Shang, C.; Wang, G.; Wei, Y.-C.; Jiang, Q.; Liu, K.; Zhang, M.; Chen, Y.-Y.; Chang, X.; Liu, F.; Yin, S.; Chou, P.-T.; Fang, Y. Excimer Formation of Perylene Bisimide Dyes within Stacking-Restrained Folda-Dimers: Insight into Anomalous Temperature Responsive Dual Fluorescence. CCS Chem. 2021, 3, 1921–1932.
- (29) Kim, W.; Nowak-Król, A.; Hong, Y.; Schlosser, F.; Würthner, F.; Kim, D. Solvent-Modulated Charge-Transfer Resonance Enhancement in the Excimer State of a Bay-Substituted Perylene Bisimide Cyclophane. *J. Phys. Chem. Lett.* **2019**, *10*, 1919–1927.
- (30) Majumdar, P.; Tharammal, F.; Gierschner, J.; Varghese, S. Tuning Solid-State Luminescence in Conjugated Organic Materials: Control of Excitonic and Excimeric Contributions through π Stacking

- and Halogen Bond Driven Self-Assembly. ChemPhysChem 2020, 21, 616-624.
- (31) Veldman, D.; Chopin, S. M. A.; Meskers, S. C. J.; Groeneveld, M. M.; Williams, R. M.; Janssen, R. A. J. Triplet Formation Involving a Polar Transition State in a Well-Defined Intramolecular Perylenediimide Dimeric Aggregate. *J. Phys. Chem. A* **2008**, *112*, 5846–5857.
- (32) Barashkov, N. N.; et al. Excimers of organic molecules. Russ. Chem. Rev. 1993, 62, 539-552.
- (33) Engels, B.; Engel, V. The dimer-approach to characterize optoelectronic properties of and exciton trapping and diffusion in organic semiconductor aggregates and crystals. *Phys. Chem. Chem. Phys.* **2017**, 19, 12604–12619.
- (34) Zuluaga, C.; Spata, V. A.; Matsika, S. Benchmarking Quantum Mechanical Methods for the Description of Charge-Transfer States in π -Stacked Nucleobases. *J. Chem. Theory Comput.* **2021**, *17*, 376–387.
- (35) Oleson, A.; Zhu, T.; Dunn, I. S.; Bialas, D.; Bai, Y.; Zhang, W.; Dai, M.; Reichman, D. R.; Tempelaar, R.; Huang, L.; Spano, F. C. Perylene Diimide-Based Hj- and hJ-Aggregates: The Prospect of Exciton Band Shape Engineering in Organic Materials. *J. Phys. Chem.* C 2019, 123, 20567–20578.
- (36) Yamagata, H.; Maxwell, D. S.; Fan, J.; Kittilstved, K. R.; Briseno, A. L.; Barnes, M. D.; Spano, F. C. HJ-Aggregate Behavior of Crystalline 7,8,15,16-Tetraazaterrylene: Introducing a New Design Paradigm for Organic Materials. *J. Phys. Chem. C* **2014**, *118*, 28842–28854.
- (37) Strong, S. E.; Hestand, N. J. Modeling nonlocal electronphonon coupling in organic crystals using interpolative maps: The spectroscopy of crystalline pentacene and 7,8,15,16-tetraazaterrylene. *J. Chem. Phys.* **2020**, *153*, 124113.
- (38) Munn, R. W.; Silbey, R. Theory of electronic transport in molecular crystals. II. Zeroth order states incorporating nonlocal linear electron-phonon coupling. *J. Chem. Phys.* **1985**, *83*, 1843–1853.
- (39) Son, M.; Park, K. H.; Shao, C.; Würthner, F.; Kim, D. Spectroscopic Demonstration of Exciton Dynamics and Excimer Formation in a Sterically Controlled Perylene Bisimide Dimer Aggregate. *J. Phys. Chem. Lett.* **2014**, *5*, 3601–3607.
- (40) Margulies, E. A.; Shoer, L. E.; Eaton, S. W.; Wasielewski, M. R. Excimer formation in cofacial and slip-stacked perylene-3,4:9,10-bis(dicarboximide) dimers on a redox-inactive triptycene scaffold. *Phys. Chem. Phys.* **2014**, *16*, 23735–23742.
- (41) Giaimo, J. M.; Lockard, J. V.; Sinks, L. E.; Scott, A. M.; Wilson, T. M.; Wasielewski, M. R. Excited Singlet States of Covalently Bound, Cofacial Dimers and Trimers of Perylene-3,4:9,10-bis-(dicarboximide)s. J. Phys. Chem. A 2008, 112, 2322–2330.
- (42) Howard, I. A.; Laquai, F.; Keivanidis, P. E.; Friend, R. H.; Greenham, N. C. Perylene Tetracarboxydiimide as an Electron Acceptor in Organic Solar Cells: A Study of Charge Generation and Recombination. *J. Phys. Chem. C* **2009**, *113*, 21225–21232.
- (43) Wirsing, S.; Hänsel, M.; Belova, V.; Schreiber, F.; Broch, K.; Engels, B.; Tegeder, P. Excited-State Dynamics in Perylene-Based Organic Semiconductor Thin Films: Theory Meets Experiment. *J. Phys. Chem. C* **2019**, *123*, 27561–27572.
- (44) Holstein, T. Studies of polaron motion. *Ann. Phys.* (N. Y). **1959**, 8, 325–342.
- (45) West, B. A.; Womick, J. M.; McNeil, L. E.; Tan, K. J.; Moran, A. M. Influence of Vibronic Coupling on Band Structure and Exciton Self-Trapping in α -Perylene. *J. Phys. Chem. B* **2011**, *115*, 5157–5167.
- (46) Coropceanu, V.; Sánchez-Carrera, R. S.; Paramonov, P.; Day, G. M.; Brédas, J.-L. Interaction of Charge Carriers with Lattice Vibrations in Organic Molecular Semiconductors: Naphthalene as a Case Study. *J. Phys. Chem. C* **2009**, *113*, 4679–4686.
- (47) Hestand, N. J.; Spano, F. C. Interference between Coulombic and CT-mediated couplings in molecular aggregates: H- to J-aggregate transformation in perylene-based π -stacks. J. Chem. Phys. 2015, 143, 244707.
- (48) Hannewald, K.; Stojanović, V. M.; Schellekens, J. M. T.; Bobbert, P. A.; Kresse, G.; Hafner, J. Theory of polaron bandwidth

- narrowing in organic molecular crystals. Phys. Rev. B 2004, 69, 075211.
- (49) Renaud, N.; Grozema, F. C. Intermolecular Vibrational Modes Speed Up Singlet Fission in Perylenediimide Crystals. *J. Phys. Chem. Lett.* **2015**, *6*, 360–365.
- (50) Gisslén, L.; Scholz, R. Crystallochromy of perylene pigments: Interference between Frenkel excitons and charge-transfer states. *Phys. Rev. B* **2009**, *80*, 115309.
- (51) Hestand, N. J.; Spano, F. C. Expanded Theory of H- and J-Molecular Aggregates: The Effects of Vibronic Coupling and Intermolecular Charge Transfer. *Chem. Rev.* **2018**, *118*, 7069–7163.
- (52) Hoffmann, M.; Soos, Z. G. Optical absorption spectra of the Holstein molecular crystal for weak and intermediate electronic coupling. *Phys. Rev. B* **2002**, *66*, 024305.
- (53) Coropceanu, V.; Cornil, J.; da Silva Filho, D. A.; Olivier, Y.; Silbey, R.; Brédas, J.-L. Charge Transport in Organic Semiconductors. *Chem. Rev.* **2007**, *107*, 926–952.
- (54) Hoche, J.; Schmitt, H.-C.; Humeniuk, A.; Fischer, I.; Mitrić, R.; Röhr, M. I. S. The mechanism of excimer formation: an experimental and theoretical study on the pyrene dimer. *Phys. Chem. Chem. Phys.* **2017**, *19*, 25002–25015.
- (55) Philpott, M. R. Theory of the Coupling of Electronic and Vibrational Excitations in Molecular Crystals and Helical Polymers. *J. Chem. Phys.* **1971**, *55*, 2039–2054.
- (56) Yamagata, H.; Pochas, C. M.; Spano, F. C. Designing J- and H-Aggregates through Wave Function Overlap Engineering: Applications to Poly(3-hexylthiophene). *J. Phys. Chem. B* **2012**, *116*, 14494–14503.
- (57) Miyazaki, M.; Fujii, M. A structural study on the excimer state of an isolated benzene dimer using infrared spectroscopy in the skeletal vibration region. *Phys. Chem. Chem. Phys.* **2017**, *19*, 22759–22776.
- (58) Wu, Y.; Zhou, J.; Phelan, B. T.; Mauck, C. M.; Stoddart, J. F.; Young, R. M.; Wasielewski, M. R. Probing Distance Dependent Charge-Transfer Character in Excimers of Extended Viologen Cyclophanes Using Femtosecond Vibrational Spectroscopy. *J. Am. Chem. Soc.* **2017**, *139*, 14265–14276.
- (59) Murrell, J.; Tanaka, J. The theory of the electronic spectra of aromatic hydrocarbon dimers. *Mol. Phys.* **1964**, *7*, 363–380.
- (60) Nowak-Król, A.; Fimmel, B.; Son, M.; Kim, D.; Würthner, F. Photoinduced electron transfer (PET) versus excimer formation in supramolecular p/n-heterojunctions of perylene bisimide dyes and implications for organic photovoltaics. *Faraday Discuss.* **2015**, *185*, 507–527.
- (61) Scholz, R.; Kobitski, A. Y.; Zahn, D. R. T.; Schreiber, M. Investigation of molecular dimers in α -PTCDA by ab initio methods: Binding energies, gas-to-crystal shift, and self-trapped excitons. *Phys. Rev. B* **2005**, 72, 245208.
- (62) Spata, V. A.; Lee, W.; Matsika, S. Excimers and Exciplexes in Photoinitiated Processes of Oligonucleotides. *J. Phys. Chem. Lett.* **2016**, *7*, 976–984.
- (63) Canola, S.; Bagnara, G.; Dai, Y.; Ricci, G.; Calzolari, A.; Negri, F. Addressing the Frenkel and charge transfer character of exciton states with a model Hamiltonian based on dimer calculations: Application to large aggregates of perylene bisimide. *J. Chem. Phys.* **2021**, *154*, 124101.
- (64) Settels, V.; Schubert, A.; Tafipolski, M.; Liu, W.; Stehr, V.; Topczak, A. K.; Pflaum, J.; Deibel, C.; Fink, R. F.; Engel, V.; Engels, B. Identification of Ultrafast Relaxation Processes As a Major Reason for Inefficient Exciton Diffusion in Perylene-Based Organic Semiconductors. *J. Am. Chem. Soc.* **2014**, *136*, 9327–9337.
- (65) Mladenovic, M.; Fink, R. F.; Thiel, W.; Schirmeister, T.; Engels, B. On the Origin of the Stabilization of the Zwitterionic Resting State of Cysteine Proteases: A Theoretical Study. *J. Am. Chem. Soc.* **2008**, 130, 8696–8705.
- (66) Frisch, M. J. et al. *Gaussian 16*, rev. C.01; Gaussian Inc.: Wallingford, CT, 2016.

- (67) Chai, J.-D.; Head-Gordon, M. Long-range corrected hybrid density functionals with damped atom-atom dispersion corrections. *Phys. Chem. Phys.* **2008**, *10*, 6615.
- (68) Weigend, F.; Ahlrichs, R. Balanced basis sets of split valence, triple zeta valence and quadruple zeta valence quality for H to Rn: Design and assessment of accuracy. *Phys. Chem. Chem. Phys.* **2005**, *7*, 3297.
- (69) Walter, C.; Krämer, V.; Engels, B. On the applicability of time-dependent density functional theory (TDDFT) and semiempirical methods to the computation of excited-state potential energy surfaces of perylene-based dye-aggregates. *Int. J. Quantum Chem.* **2017**, *117*, e25337.
- (70) Lu, T.; Chen, F. Multiwfn: A Multifunctional Wavefunction Analyzer. J. Comput. Chem. 2012, 33, 580-592.
- (71) Becke, A. D. Density-functional thermochemistry. III. The role of exact exchange. *J. Chem. Phys.* **1993**, *98*, 5648–5652.
- (72) Dunning, T. H. Gaussian basis sets for use in correlated molecular calculations. I. The atoms boron through neon and hydrogen. *J. Chem. Phys.* **1989**, *90*, 1007–1023.
- (73) Valeev, E. F.; Coropceanu, V.; da Silva Filho, D. A.; Salman, S.; Brédas, J.-L. Effect of Electronic Polarization on Charge-Transport Parameters in Molecular Organic Semiconductors. *J. Am. Chem. Soc.* **2006**, *128*, 9882–9886.
- (74) Mooney, J.; Kambhampati, P. Get the Basics Right: Jacobian Conversion of Wavelength and Energy Scales for Quantitative Analysis of Emission Spectra. J. Phys. Chem. Lett. 2013, 4, 3316–3318.
- (75) Zubiria-Ulacia, M.; Matxain, J. M.; Casanova, D. The role of CT excitations in PDI aggregates. *Phys. Chem. Chem. Phys.* **2020**, 22, 15908–15918.
- (76) Yoo, H.; Yang, J.; Yousef, A.; Wasielewski, M. R.; Kim, D. Excimer Formation Dynamics of Intramolecular π -Stacked Perylene-diimides Probed by Single-Molecule Fluorescence Spectroscopy. *J. Am. Chem. Soc.* **2010**, *132*, 3939–3944.
- (77) Hong, Y.; Kim, J.; Kim, W.; Kaufmann, C.; Kim, H.; Würthner, F.; Kim, D. Efficient Multiexciton State Generation in Charge-Transfer-Coupled Perylene Bisimide Dimers via Structural Control. J. Am. Chem. Soc. 2020, 142, 7845–7857.
- (78) Coleman, A. F.; Chen, M.; Zhou, J.; Shin, J. Y.; Wu, Y.; Young, R. M.; Wasielewski, M. R. Reversible Symmetry-Breaking Charge Separation in a Series of Perylenediimide Cyclophanes. *J. Phys. Chem.* C 2020, 124, 10408–10419.
- (79) Fang, S.; Zhou, J.; Zhou, X.; Wang, C.; Jiang, N.; Liu, L.; Xie, Z. Interchromophore Rotation-Related Ultrafast Charge Separation at Excited States in Head-to-Tail Linked Perylene Diimide Dyads. *J. Phys. Chem. C* **2019**, *123*, 23306–23311.
- (80) Alzola, J. M.; Tcyrulnikov, N. A.; Brown, P. J.; Marks, T. J.; Wasielewski, M. R.; Young, R. M. Symmetry-Breaking Charge Separation in Phenylene-Bridged Perylenediimide Dimers. *J. Phys. Chem. A* **2021**, *125*, 7633–7643.
- (81) Giaimo, J. M.; Gusev, A. V.; Wasielewski, M. R. Excited-State Symmetry Breaking in Cofacial and Linear Dimers of a Green Perylenediimide Chlorophyll Analogue Leading to Ultrafast Charge Separation. J. Am. Chem. Soc. 2002, 124, 8530–8531.
- (82) Katoh, R.; Katoh, E.; Nakashima, N.; Yuuki, M.; Kotani, M. Near-IR Absorption Spectrum of Aromatic Excimers. *J. Phys. Chem. A* **1997**, *101*, 7725–7728.
- (83) Mauck, C. M.; Young, R. M.; Wasielewski, M. R. Characterization of Excimer Relaxation via Femtosecond Shortwave- and Mid-Infrared Spectroscopy. *J. Phys. Chem. A* **2017**, *121*, 784–792.

□ Recommended by ACS

Super-Excimer: Anomalous Bonding in a Metastable Excited-State Dimer of Superatomic Dimers

Wanrong Huang, Zhigang Wang, et al.

SEPTEMBER 02, 2022

THE JOURNAL OF PHYSICAL CHEMISTRY LETTERS

READ 🗹

Probing Through-Bond and Through-Space Interactions in Singlet Fission-Based Pentacene Dimers

Ashish Sharma, Girish Lakhwani, et al.

SEPTEMBER 23, 2022

THE JOURNAL OF PHYSICAL CHEMISTRY LETTERS

READ 🗹

Intermolecular Charge Transfer in H- and J-Aggregates of Donor-Acceptor-Donor Chromophores: The Curious Case of Bithiophene-DPP

Xin Chang, Frank C. Spano, et al.

OCTOBER 28, 2022

THE JOURNAL OF PHYSICAL CHEMISTRY C

READ 🗹

Origins of Molecular-Twist-Triggered Intersystem Crossing in Functional Perylenediimides: Singlet-Triplet Gap versus Spin-Orbit Coupling

Raka Ahmed and Arun K Manna

SEPTEMBER 14, 2022

THE JOURNAL OF PHYSICAL CHEMISTRY A

READ 🗹

Get More Suggestions >